Asymmetrical Mass Considerations on the Motion of Planing Vessels

Li P. Sung

A dissertation
submitted in partial fulfillment of the
requirements for the degree of

Doctor of Philosophy

University of Washington

2021

Reading Committee:

Brian Fabien, Chair

Alberto Aliseda

Steve Brunton

Dana Dabiri

Program Authorized to Offer Degree:
Department of Mechanical Engineering

University of Washington

Abstract

Asymmetrical Mass Considerations
on the Motion of Planing Vessels

Li P. Sung

Chair of the Supervisory Committee:
Dr. Brian Fabien
Affiliate Professor, Department of Mechanical Engineering, University of Washington

Recent advances in planing unmanned surface vessels (USV) have renewed interest in motion control, particularly related to transverse instabilities. We propose a novel method to affect maneuver and seakeeping motion by using inertial mass distribution within the vessel hull, in the volume normally occupied by passengers. This requires development of a control oriented model. However, unlike displacement vessels, roll and yaw coupled dynamics in planing vessels must be considered. In this study, we provide a first principles based analysis of these dynamics to establish a reduced order non-linear maneuvering model for prismatic planing hulls in calm water. Using this model, we show that optimized asymmetrical mass distribution yields drag savings of up to 10% with improved stability on a turning maneuver. In addition, we demonstrate the advantages of optimal feedback control using an inertial mass in seakeeping applications over traditional rudder methods.

Roll yaw coupled dynamics are not well characterized and existing low cost models are limited in range of applicability. We utilize an interpolation based approach augmented with empirical equations to address a wider range of conditions with reduced computational requirements. By interpolating test data to estimate hydrodynamic forces and empirically modeling roll damping and added mass, we establish a four degree of freedom (4DOF) maneuvering model for prismatic planing hulls in calm water with fixed asymmetrical loading.

It is validated against relevant tests and show significant computational resource savings in comparison with potential flow based methods. Simulation of an extreme turning maneuver and an asymmetrical loading case demonstrates its potential for use in initial design, control and evaluation.

This model is able to capture the hydrodynamic sensitivities to attitude parameters such as deadrise, heel, and trim angle. These effects are exploited to achieve maneuvering objectives. Demonstrated through numerical model-based simulations, asymmetrical mass distribution on low deadrise hulls affects heel and induce yaw moments that turn the vessel without the use of traditional aft steering mechanisms. On high deadrise hulls, maneuvering by use of a combined rudder and asymmetrical mass results in 10% drag savings and improved stability in comparison with rudder alone.

To consider feedback control of an inertial mass free to move laterally within the hull, additional dynamics are added using a Lagrangian approach to make a 5DOF model. Through numerical simulations, we demonstrate roll control of planing vessels using optimal feedback control. A Linear Quadratic Regulator is implemented to maintain a steady trajectory in the presence of wave disturbances and performance is compared against a rudder roll stabilizer. The results as shown in linear analysis and nonlinear time domain simulation indicate that a mass weighing 10% of vessel weight can achieve a disturbance rejection of greater than 10 dB over rudder stabilization methods and eliminates an undesirable non-minimum phase behavior characteristic of rudder systems. Due to the roll yaw force coupling of planing vessels, such inertial mass methods can be utilized to meet both seakeeping and maneuver objectives and eliminate the need for external fin type control mechanisms such as a rudder.

TABLE OF CONTENTS

LIST OF FIGURES

GLOSSARY

A: Mass matrix

b: beam

B: Damping matrix

C_{RB}: Rigid body centripetal matrix

D: Damping matrix

F: External force matrix

F_{HD}: Hydrodynamic forces

F_{CONT}: Control forces

F_D: Active actuation force applied on the inertial mass

F_{RUD}: Forces from rudder

F_{MASS}: Forces on vessel-inertial mass system due to the inertial mass

F_∇: Volumetric Froude number

I: Vessel moments of inertia about respective axis denoted in subscript

F_{HD}: Hydrodynamic forces

K, N: Moments (lbf/ft) in roll and yaw

K_{INT}, N_{INT}: Interpolated values accounting for roll restoring and yaw damping moments (lbf/ft)

K_{AM}, N_{AM}: Forces due to added mass in roll and yaw (lbf)

$K_{\dot{P}}$: Added mass due to roll in roll direction (slugs)

K_R, N_R: Roll and Yaw moments due to rudder (lbf-ft)

lcg: Longitudinal center of gravity in ft from transom

lcg_{ref}: Reference longitudinal center of gravity prior to mass shift in ft from transom

loa: Vessel length overall (ft)

m_a: Mass representing asymmetrical loading (slugs)

m_b: Vessel mass (slugs)

$N_{\dot{V}}$, $N_{\dot{R}}$: Added mass due to sway and yaw in yaw direction

N_ϕ: Maneuvering derivative – Heel induced yaw moment

p,r: Roll and Yaw rate (°/s)

STD: Steady turning diameter (ft)

u,v: Forward and side velocity, body frame (ft/s)

x,y: Position, inertial frame (ft)

vcg: Vertical center of gravity (ft)

z_0: Vertical distance between inertial mass and vcg (ft)

X, Y: Forces (lbf) in surge and sway

X_{INT}, Y_{INT}: Interpolated values accounting for damping forces

X_{AM}, Y_{AM}: Forces due to added mass in surge and sway

$X_{\dot{U}}$: Added mass due to surge in surge direction

$Y_{\dot{V}}$, $Y_{\dot{R}}$: Added mass due to sway and yaw in sway direction

δ: Angle of waterjet flow deviating from directly aft $^\circ$

η: Velocity vector

ν: State vector

τ: Trim angle $^\circ$

ϕ, ψ: Roll and heading angles, inertial frame $^\circ$

ACKNOWLEDGMENTS

The author would like to thank his advisor, Dr. Brian Fabien, for his dedication and commitment, Dr. Carolyn Judge and Dr. Michael Morabito of the US Naval Academy for their generous time and advice, and to the US Navy Permanent Military Professor Program for this study opportunity and academic freedom.

DEDICATION

to my dear wife Ione, and daughters Iona and Tayana

Chapter 1
INTRODUCTION

The introduction section, we seek to orient the reader to the subject of the thesis, a review of previous revelevant material, and provide the objective and overview of this study.

1.1 Background

Advances in robotics have ushered a proliferation of high-speed Unmanned Surface Vessels (USV)s which are uniquely suited to tasks such as exploration and environmental monitoring. Planing dynamics enables them to respond quickly to sudden emerging environmental event of interest, track fast moving fish, or pursue illegal activity. Because these vessels do not have a requirement for personnel berthing, they can be relatively low cost and small. However, they are constrained by their energy carrying or harvesting limitations, motivating designers toward energy efficient operations. In addition, stability in the presence of environmental disturbances is a desirable trait. In order to operate at high speeds, instabilities must be identified and control strategies develop to provide margin from these instabilities. However, transverse instabilities are not well characterized. For example, for causes for end swap instabilities that have caused casualties in shallow bottom boats [45] have caused casualties and empirically observed [5] but not well understood. Improve characterization of these instabilities are required to increase performance.

Two essential tasks for such a vessel platform are: 1) maneuver, or the movement on the x-y horizontal plane and 2) seakeeping, which is traditionally the ability to maintain a fixed position or a straight trajectory. Operating directional sonar, telemetry, or communications equipment requires steadiness within tolerance constraints. In contrast with maneuvering, the seakeeping problem is one of disturbance rejection on the vertical plane. These forces

consist of heave, roll, and pitch, which are translation in z, and rotation about x and y. Vessels are generally more susceptible to unwanted motions in roll since their transverse moments of inertia are relatively small compared to longitudinal moments of inertia.

New (USV)s coming onto market are relatively small. 60% of them are less than 23' in length. Lithium batteries are a main source of power, which can occupy a large fraction of the overall mass budget. Traditionally, they would use controllable transom fins such as rudders for maneuver and seakeeping control. However, the absence of personnel carrying requirement aboard USV may give it the unique ability to actively move the location of the battery within the body of the vessel, which may exploit coupled roll and yaw forces to support maneuver or seakeeping objectives. A familiar example is the surfboard, where active distribution of the rider's body weight helps establish desired trajectories in the planing dynamic regime. Using mass distribution on a USV for maneuver may reduce the requirement for a rudder, providing shallower draft for greater area access and valuable drag reduction for greater duration at sea. Such an actuator can be completely enclosed within the vessel to reduce the risk of corrosion, fouling and damage in comparison to a traditional external steering mechanism. For seakeeping, small vessels that perform survey, directed energy, or communications tasks may desire reduced roll motion. Movement of the battery mass within the vessel could provide roll moments to counter act environmental disturbances. However, active inertial mass actuation for roll damping on small planing maritime vessels is a relatively unexplored topic. It would require control-oriented modeling to assess the hydrodynamic effects on a vessel due to time varying inertial mass position and changes in moments of inertia.

In comparison to displacement type vessel hulls that rely on buoyancy for support, hulls in the planing dynamic regime use the vessel's forward velocity and angle of attack to generate lift. This adds complexity to the modeling effort. Sea spray, wake, multiphase fluids effects of air and water, undulating surface waves, coupled forces between horizontal and vertical planes, sharp angles found on modern planing hulls, and associated flow separation are just a few of such difficulties. Study of displacement vessels generally assume decoupled vertical and

horizontal plane forces [69] [68]. This would be an oversimplification for planing vessels since roll forces are highly coupled with yaw. A modeling method is desired that can capture the maneuvering and seakeeping characteristics of planing vessels, yet simple enough to provide quick processing for stability analysis and control development.

Due to the mentioned complexities, horizontal plane instabilities of planing hulls are yet to be fully characterized. An example of an instability that is caused by complex dynamics not found on displacement vessels is shown in shallow-draft boat spinouts [1]. Morabito indicates that the potential for excessive roll during a turning maneuver to induce ventilation to the propeller, causing rapid deceleration, drop in pitch, high yaw moment and a loss of control. Since planing hulls are highly sensitive to parameters such as roll, this further motivates our study on roll control as a means of instability avoidance.

Traditionally, high speed vessels use hydrodynamic means to affect motion, such as a steering mechanism of a rudder, transom flaps, or directional thrust jets. However, these external appendages are exposed to hydrodynamic drag forces that act against vessel's intended course. It is desired to minimize the energy required to overcome such drag since performance and mission duration is affected. In addition, rudders and external steering mechanisms are exposed to often harsh environments, susceptible to fouling, corrosion, and damage. A method of maneuver that does not incur drag or require such moving parts may extend an autonomous vessel's life at sea. A rudder or external fin appendage may also affect a vessel's overall draft. Rudders are one of the lowest parts on a planing vessel since rudder fluid immersion is required for operation and may prevent access to shallow areas of interest.

We seek to uncover methods of active distribution of inertial mass to exploit the roll-yaw coupling of planing vessels to affect both roll control and turning, conceptually similar to a surfer on a surfboard. Methods that can meet both seakeeping and maneuver objectives would eliminate the need for traditional external fin type control mechanisms such as a rudder. That can be advantageous in drag reduction, allowing shallow water access, and in other situations that disfavor rudders.

1.2 Review of Modeling Methods

Numerically modeling the hydrodynamic forces of planing vessels is a complex challenge. Multi-phase fluid interactions between air and water, sea spray, wake effects, undulating wave surface, coupled dynamics between horizontal and vertical planes, and sharp angles found on modern planing hulls causing flow separation are just a few of such difficulties. Previous studies have employed various approaches such as high-fidelity Computational Fluid Dynamics (CFD), potential flow-based theory, empirical equations, and interpolation of test data. However, low-cost maneuvering modeling that can be easily linearized and quickly simulated does not yet exist to support development of new controls and optimization methods. This approach was used by researchers such as Xi, Sun [65] and Sakaki [53] to address porpoising in the heave and pitch dimensions. In this paper, we extend this philosophy and develop a simplified approach to the full non-linear dynamics to focus particularly on roll-yaw coupled dynamics. Improving the characterization of this dynamic opens the potential of using asymmetrical mass distribution to turn a vessel without a rudder like a surfer leaning into a turn.

High fidelity approaches such as CFD are time and cost prohibitive for conducting quick initial design. Low-cost modeling approaches can be classified in general categories: Empirical, 2D+t, and interpolative. Each has their own strengths and weaknesses. We propose a generalizable approach that utilizes the strengths of each type of model. This method results in the ability to quickly simulate a wider range of trajectories than any individual model type and can be scaled to accommodate improved experimental data and empirical developments as they become available. It is suitable for initial design and control applications where speed and range are key.

1.2.1 Empirical modeling background

Early work in modeling planing vessels used an empirical approach. Savitsky develop useful developed nonlinear empirically based model equations describing straight trajectories, with

the range validity of trim angles between 3° and 15° [55]. Lewandowski studied roll stability and considered the relationship of roll force to deadrise, vessel loading, rudder forces, and VCG [39]. This work was continued with methods compiled into an influential book [38]. Judge provided empirical contributions for heeled vessels with models of wetted water lengths to heel angle, lift forces, and roll moments [33] [31]. Empirical methods are accurate and quick to model certain elements of maneuver such as overall drag, rudder effects [27], but lack the ability to accurately capture the broad range of effects of roll, sway, yaw coupling needed to produce a complete maneuvering model.

1.2.2 History and assumptions of 2D+t approach

Influential early development of models introducing low aspect ratio strip theory with potential flow methods was published [70] considering vessels in straight symmetrical trajectories. Incompressible and inviscid fluid are the underlying assumptions of potential flow theory not accounting for such effects of flow separation and eddies. Theory was augmented by empirical means such as development of factor to account for aft suction and near-transom lift [24]. To model planing hull maneuver, oblique and asymmetric movement through fluid medium must be considered. A model of oblique water entry of an asymmetrical wedge utilizing BEM was mathematically developed by Xu [66]. This work is continued considering rotation of wedge [67]. Oblique theory was improved in evaluation with experimental data in [44] [46] [47]. Tavakoli used these theories in simulation of PMM tests and 6DOF planing maneuvers [61] with accurate results limited to trajectories within 0° to 10° in roll and yaw, and positive trim angles. Outside of that range, inaccuracies arise due to flow separation, lateral flow under keel, and other nonlinear viscous effects that violate underlying assumptions. Algarin performed 6DOF simulation of a turning maneuver using 2D+t slender body theory and tested the results against CFD [2]. Simulated maneuvers included turning circle and zig zags, within 10 degrees in roll angle, and results showed accuracy against CFD. Simulated trajectories observed the same range limits as described by Dashtimanesh.

Recent developments in oblique and asymmetric two-dimensional wedge impact predic-

tions have improved the applicability of potential flow based methods. However, the high angles of roll, crossflow, or negative angles of attack that characterize extreme transverse plane maneuvers have yet to be adequately addressed.

1.2.3 Interpolation based modeling background

Early interpolation models fit linear models or Taylor series representation of hydrodynamic forces using maneuvering derivatives fits from Planar Motion Mechanism (PMM) tests [1]. More recent work along this line employ modern system ID or vector regression techniques [41]. However, these models do not capture non-linearities of planing hydrodynamics which reduces their applicability at larger deviations as noted [33]. Each model is unique to a particular hull shape and not generalizable. Katayama tests in the 2000's developed into a full interpolation based 3DOF maneuver model [35] of a unique hull shape. Limitations of the Katayama 3DOF model are the inability to independently consider changes in heel or pitch. These models were expanded to higher DOF; Data from sea trials was used to establish hydrodynamic coefficients for a 6DOF model [30]. However, like other interpolation-based models, this approach only considers a single vessel design and is not generically adaptable to a broader range of hulls. This motivates a blended approach that takes advantage of the strengths of each model type. Using a generic dataset and estimating hydrodynamic forces based on interpolation between geometric hull parameters as well as state variables, a model can apply to a broader range of vessels and can be used for optimization and control development. This parametrized approach offers advantages from previous interpolation-based models in applicability. Utilizing interpolation-based modeling can better simulate extreme maneuvers as test data is available and is not encumbered to the limited range of 2D+t methods. Also, it eliminates the need to apply correction factors that complicate 2D+t methods, reducing computational requirements and provide speed advantages over existing methods. Kinematics can account for changes in operating condition such as movement of mass during a trajectory, not previously considered, and thus provide useful approaches to evaluating new dynamics involving asymmetrical mass distribution.

1.3 Review of Actuation Methods

Across engineering disciplines, mass distribution to support motion control is not a new concept. In structural engineering, we find such systems at the top of tall buildings where pendulum masses counter resonance to reduce motion. Heidari proposed a LQR-PID application to Active Tuned Mass Dampers (ATMD) with a cuckoo search optimization algorithm on simulated buildings in historical earthquakes. On land, skateboards, snowboards, segways, and hoverboards all use active mass actuation to influence motion. This is similarly found in board sports on water, such as surfing, wakeboarding, foiling boards, etc... In larger maritime craft, Anti-Roll Tanks (ART) use fluid in internal tanks to counter roll motion [37]. The ART concept was introduced in the late 1800's but not widely implemented. Linear motion mass actuation with a magnetic levitating system for motion control was explored by [48]. Finally, in aerospace applications, active mass distribution is effective rotational motion control for re-entry vehicles where high velocities make traditional external fin appendages impractical, Erturk [18] [19] explored the use of active mass actuation in aircraft to influence the pitch and roll moments.

To develop roll control, we can find relevant studies in seakeeping theory where the objective is to maintain a trajectory to a steady heading and avoid instabilities in the presence of environmental disturbances. Of fin-based seakeeping methods, rudder roll stabilization (RRS) has been extensively studied. The advantage of these systems are that do not require much additional space or weight since they use the same mechanism to achieve both maneuvering and seakeeping objectives. A drawback is the requirement for differential velocity across the rudder. This method inherently poses drag that is exponentially larger at high speeds and is not effective when the vessel as at low speeds.

Inertial based motion control systems do not suffer such drawbacks. A simple example is a surfer that manipulates the inertial properties of his or her body through the forces transmitted from foot to a planing surfboard. Controls are developed through learned experience to address stability and maneuver. More relevant to the maritime industry are examples of

Active Roll Tanks (ART) and gyro stabilizers, both of which requiring potentially substantial mass budget and volume within the vessel. The smallest gyro stabilizers weigh around 360 lbs; however, 60% of new USV on the market are less than 23' in length [8] and are not likely to dedicate the mass budget to utilize these stabilization methods. The advantages of inertial based motion control motivate the study of methods not previously identified.

A few researchers have studied the use of a passive spring mass damper type system aboard displacement vessels to mitigate roll. The concept of using moving a solid mass linearly across a vessel's lateral axis for roll disturbance rejection was studied by Montazeri [9] who modeled a on a displacement vessel and Ayob [3] specifically for a 22' fishing boat. Shekhtman [10] applied a similar concept to a rotating pendulum and modeled a displacement vessel-pendulum system in a seven degree of freedom (7DOF).

Of active control methods, Su [57] explored fuzzy sliding-mode controller on a mobile wheeled platform as a test platform for roll motion control of ships. Li studied Sliding Mode Control (SMC) [40] and Santoso applied Fuzzy Gain Scheduling (FGS-PID) [54] to for RRS

This motivates the development of an inertial mass – vessel system with active feedback to support both maneuver and seakeeping objectives.

1.4 Objective and Overview

We propose a 1st principles-based approach that utilizes data interpolation techniques and empirical relations to provide a low-cost model for prismatic planing hulls, insight to coupled maneuver and seakeeping dynamics, and explore new possibilities of control. This will be approached in this paper through modeling, simulation, analysis, and control development. We establish a four degree of freedom (4DOF) maneuver model considering hydrodynamic effects of asymmetrical mass distribution on a prismatic planing hull including rudder dynamics. Results are validated compared with relevant tests which demonstrate the model's potential in control analysis. We further simulate an extreme turning maneuver that this model is uniquely capable to quickly simulate, and demonstrate the potential for using this model to explore novel maneuvering methods by simulating asymmetrical mass distribution

effects on maneuver, similar a surfer. Analysis is conducted based on drag, stability, and responsiveness to optimize vessel attitudes given a desired turning trajectory.

Next, we offer an extension to traditional seakeeping theory in the study of planing vessels maintaining steady turning yaw rates, vice a constant heading on a displacement vessel. We propose a novel Active Mass Actuator (AMA) with optimal feedback control for roll motion control of a prismatic planing hull. A solid mass weighing 10% of vessel is considered representative of a lithium battery aboard a small USV. It is modeled with the freedom to move laterally within the vessel on a straight track establishing a 5DOF system with the vessel hull. The system is linearized about a steady turning equilibrium, analyzed for stability and optimal feedback via a Linear Quadratic Regulation (LQR) is applied. In order to evaluate the performance of an AMA in comparison to a Rudder Roll Stabilizer (RRS), we develop dynamic models of both AMA and RRS systems. Finally, we compare and evaluate performance of both RSS and AMA using both linear analysis and nonlinear time domain simulation. We demonstrate the ability for active mass distribution to maneuver and maintain roll stability without a rudder, introducing the possibility of eliminating the requirement for external fins from the design of small planing vessels.

Chapter 2

EQUATIONS OF MOTION FOR PRISMATIC PLANING HULLS

In this section, we first establish the coordinate reference and kinematics. Dynamics are then described through empirical empirical equation and interpolation of relevant test results. As a general approach, simplifications will be implemented to reduce the computational cost while retaining the essential planing dynamics. Our intended use of this model is 1) to be linearized about an equilibrium state for analysis and control development and 2) to simulate trajectories assessing non-linear dynamics. Let $\bar{\nu}$ represent an equilibrium state $\bar{u}$ the fixed input positions associated with that equilibrium. Our objective is to develop low cost model f such that the matrices A_{lin} and B_{lin} can be quickly obtained by performing Jacobians numerically about that equilibrium.

$$A_{lin} = \frac{\partial f}{\partial \nu}|_{\bar{\nu},\bar{u}},\ B_{lin} = \frac{\partial f}{\partial u}|_{\bar{\nu},\bar{u}} \tag{2.1}$$

This would set up our desired continuous time linear time-invariant system.

$$\dot{\nu} = A_{lin}\nu + B_{lin}u \tag{2.2}$$

2.1 Coordinates and Equations of Motion

A turning maneuver model traditionally considers the three degrees of freedom (3DOF) necessary to describe trajectories on the transverse plane: surge, sway, and yaw. To study

the roll-yaw coupled dynamic, a degree of freedom in roll is additionally required. To simplify the model to allow our focus on the roll-yaw coupled dynamic, heave and pitch are treated as constant. In addition, dynamics are considered only for a single fixed velocity in the fully planing regime while surge is accounted for to calculate the vessel's inertial position. These simplifications result in a 4DOF with fixed forward velocity and enable more effective assessment of asymmetrical mass loads effects on roll on maneuver.

A right-handed coordinate system is defined in Fig. 1 for the prismatic planing vessel running in calm water with the origin about the nominal center of gravity. At the equilibrium running attitude, the trim angle is defined as τ, heel as ϕ, yaw heading as ψ, with forces of thrust, yaw, roll, and sway as X, Y, K, N respectively.

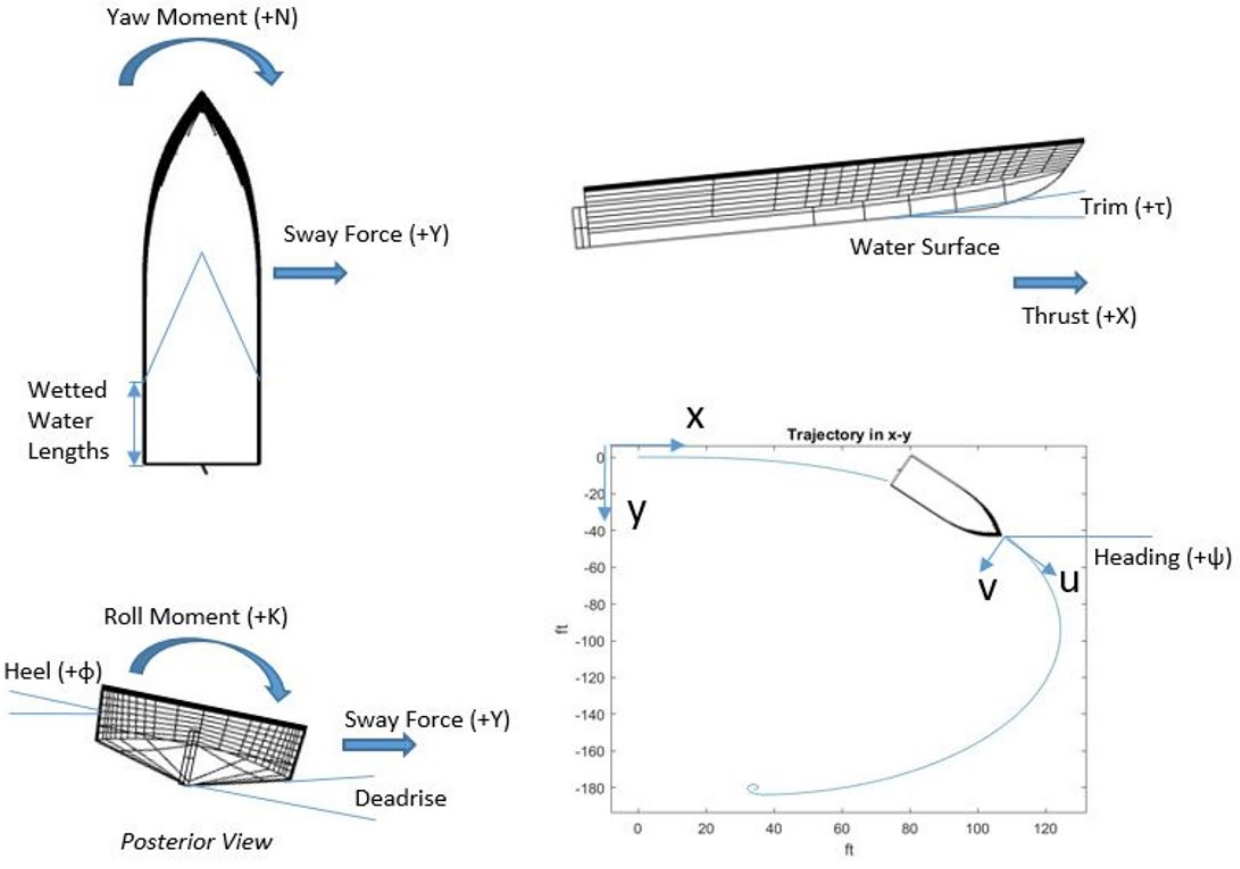

Figure 2.1: Coordinate System: Right handed coordinate system indicates positive direction

To establish equations of motion in state form, we establish matrices for rigid body centripetal terms, mass, damping, hydrodynamic force, and control forces with methods described in [23]. Control inputs are accounted for separately with the end goal in mind.

2.1.1 Interpolation based modeling

We propose interpolating static drift test data and augmenting with added mass and damping models. This would enable applicability to the range of available test data and limits of the underlying empirical models. We select a comprehensive set of drift tests on prismatic hulls of various deadrise such as test results from static and rotating drift tests by [8] that captures the hydrodynamic restoring and damping forces of u, v, ϕ, and r states. Note the only state that has an associated restoring force is roll ϕ since x, y, and ψ directions have rigid body motions without an associated restoring force. Interpolation of test data provides an estimate of these hydrodynamic forces. This data allows parametric based evaluation and enables modeling across a range of prismatic hulls varying between 10° and 20° deadrise and within the bounds of test data selected. This approach broadens the applicability, in comparison with models of Katayama or Jeon where consideration was given only to a particular hull design.

Forces that are not able to be interpolated from static drift tests are those due to roll velocities or acceleration. Those must be accounted for separately in the equations of motion. Empirical expressions for added mass with cross coupled terms for sway and yaw are based on strip theory methods and follow the methods as compiled by Lewandowski [38].

The Brown & Klosinski (B&K) measurements were taken at the fixed point where the gantry assembly attached to the test vessel. Forces experienced at that point first require adjustment to what a free body vessel would experienced based on the distance between the measurement point and the modeled lcg. Using B&K test data in an interpolative fashion allows consideration of vessel dynamics outside of the range of current empirical theory application.

Because pitch is not a state in our 4DOF model, trim angle is treated as a constant

with dependency on lcg using Savitsky methods [55]. Assuming steady state, we can apply Savitsky empirical equations in force balance to solve for hydrodynamic characteristics as summarized in the follow procedure. In steady state pitch moment balance, lcg must be coincident with the hydrodynamic center of pressure on the hull. This allows us to solve the following equation numerically for wetted water length to beam ratio λ.

$$\frac{lcg}{\lambda b} = .75 - \frac{1}{5.21\frac{C_V^2}{\lambda^2} + 2.39} \tag{2.3}$$

In heave force balance, the vessel's weight is equal and opposite to lift force. This allows us to solve for the overall coefficient of lift.

$$C_{L\beta} = \frac{\Delta}{\frac{1}{2}\rho u^2 b^2} \tag{2.4}$$

Empirical relation allows us to numerically solve for a zero-deadrise surface coefficient of lift

$$C_{L\beta} = C_{L0} - .0065\beta C_{L0}^{.6} \tag{2.5}$$

We can finally arrive at steady state trim angle using an empirical relations with the coefficient of lift for a zero-deadrise surface, noting applicability from $.6 < C_v < 13$, $2 < \tau < 15$ and $\lambda < 4$

$$C_{L0} = \tau^{1.1}[.012\lambda^{\frac{1}{2}} + \frac{.0055\lambda^{\frac{5}{2}}}{C_V^2}] \tag{2.6}$$

With states determined, we can use MATLAB to perform a Delaunay triangulation that interpolates between 5 variables of angles of deadrise, heel, trim, sway velocity, and yaw rate as shown in the flowchart on Figure 2.2 and coded in Appendix E. Instead of using the MATLAB INTERPN or GRIDTANN functions to interpolate in n-dimension at every time step to attain estimated hydrodynamic force values, the interpolation tables and simplexes were pre-calculated and loaded into the MATLAB workspace at the beginning for use during the rest of the routine. This allows the computationally intensive part of the routine to be performed once instead of at every time step resulting in speeds as listed in section 4.1. This provides an estimated force within the range of data used. The process as written in

MATLAB code are shown in Appendix G with a link to a GITHUB repository in Appendix A

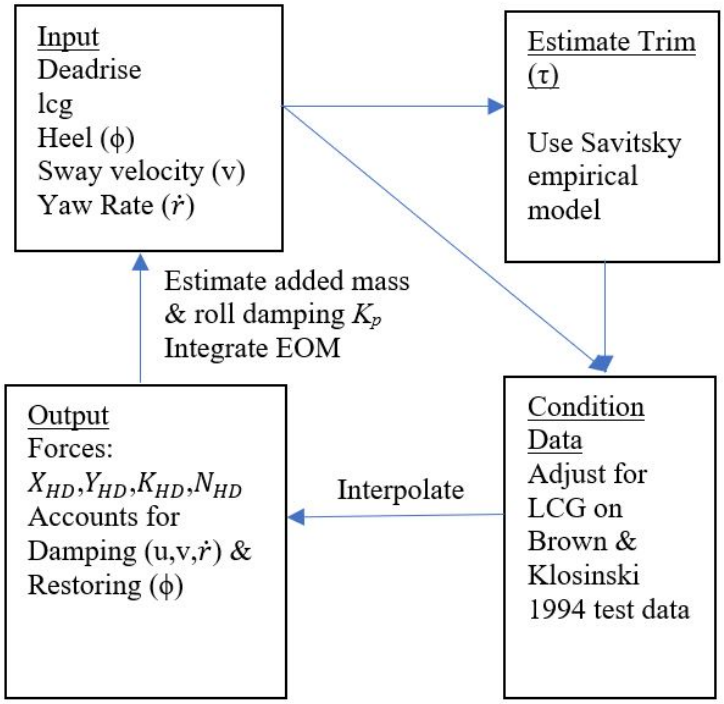

Figure 2.2: Modeling Flow Chart: Estimating hydrodynamic forces along model trajectory using interpolation of test data adjusted to account for the modeled free body lcg and empirical models for roll damping and added mass

Since static drift tests do not involve rolling motion, roll damping force is not measured in the test results of [8] and cannot be assessed simply through interpolation. This force is measured and empirical modeled in a subsequent study [9]. Thus, hydrodynamic roll force is attained by summing of the empirical roll damping force and the interpolated estimate which accounts for restoring force.

$$F_{HD} = \begin{bmatrix} X_{HD} & Y_{HD} & K_{HD} & N_{HD} \end{bmatrix}' \tag{2.7}$$

The vector consists of forces acting in thrust (X), sway (Y), roll (K), and yaw (N) that will be used in section 2.2. This provides an estimate of the hydrodynamic forces vessel but since static drift tests do not consider acceleration, added mass must be separately considered. This captures our general approach in establishing dynamics with added mass addressed in section 2.1.2 . We identify what our B&K data can accurately model in terms of our equation of motion and what must be augmented from other models.

2.1.2 Added mass and roll damping

Different approaches toward added mass modeling entails different computational requirements. Analytic approaches include potential flow based models, BEM, and RANS. Recent work in potential flow based theory include Ghadimi and Tavakoli [25] [63] with the approach summarized in work such as [56]. Potential flow based commercial codes are available, such as Powersea or WAMIT. General Hydrostatics (GHS) is another potential due to recent improved capability in dynamic stability. Castro-Feliciano [12] demonstrated co-design of vessel geometries and control using Powersea. Ticherfatine [64] also uses constant values in a control application of heave-pitch motion, though they are determined through CFD.

Added mass can be experimentally determined. Tascon [60] attained added mass and damping models by performing harmonic analysis with a fourier series using results from Judge at the US Naval Academy[33]. Xi and Sun, in development of control applications to address porpoising in heave-pitch, used experimental data to determine constant values for added mass and damping [65].

The lowest cost method is using a simply parametric rough estimate. Montazeri [43] in roll analysis for control application of a displacement vessel estimates added mass as approximately 20-25% of vessel mass.

Control oriented efforts have generally favored simplified approaches toward added mass and damping due to computational cost. This involves constant or linearized values. Because we are focusing on coupled dynamics of planing vessels, we seek expressions that also reflect that degree of coupling. However, we are also seeking a low cost approach that can

be processed quickly for development control and optimization purposes. The methods of Lewandowski [38] are established on a semi-empirical and potential flow basis. This approach captures the coupling dynamic and is relatively low cost in implementation. They are dependent on the mean metric of vessel surface in contact with the water as evidenced in the L_C, L_K, and wetted chine beam terms. For our intended purposes of performing stability analysis and controls using linearized systems, we may treat added mass and roll damping terms as time invariant about a mean equilibrium trajectory. This has the benefit of capturing the dynamic coupling effects while keeping computational costs low.

Equations of motion [39], treated with the vessel's rigid body force component segregated from the added mass component.

$$X = m\left(\dot{u} - vr\right) + X_{am} \tag{2.8}$$

$$Y = m\left(\dot{v} + ur\right) + Y_{am} \tag{2.9}$$

$$K = I_{xx}\dot{p} - I_{xz}\dot{r} \ + K_{am} \tag{2.10}$$

$$N = I_{zz}\dot{r} - I_{xz}\dot{p} + \ + N_{am} \tag{2.11}$$

Empirical expressions for added mass with cross coupled terms for sway and yaw are based on strip theory methods and follow the methods outlined in [38] on the basis of Brown and Klosinski tests on added mass and damping of planing vessels in roll [9]. Steps are summarized below.

$$X_{am} = X_{\dot{u}}\dot{u} \tag{2.12}$$

$$Y_{am} = Y_{\dot{v}}\dot{v} + Y_{\dot{r}}\dot{r} \tag{2.13}$$

$$K_{am} = K_{\dot{p}}\dot{p} \tag{2.14}$$

$$N_{am} = N_{\dot{v}}\dot{v} + N_{\dot{r}}\dot{r} \tag{2.15}$$

Sway component of sway added mass. β is deadrise angle measured in degrees, $k(\beta)$ is the hull added mass function defined in 2.21

$$Y_{\dot{v}} = -b^2\rho\tan(\beta)k(\beta)[L_K + 2L_C]/12 \tag{2.16}$$

Sway component of yaw added mass

$$N_{\dot{v}} = -b^2\rho\tan(\beta)k(\beta)[L_K^2 + 2L_K L_C + 3L_C^2]/48 \tag{2.17}$$

Yaw component of yaw added mass

$$N_{\dot{r}} = -b^2\rho\tan(\beta)k(\beta)[L_K^3 + 2L_K^2 L_C + 3L_C^2 L_K + 4L_C^3]/120 \tag{2.18}$$

Roll component of roll added mass

$$K_{\dot{p}} = -.010237\rho b^5\lambda(1 - \sin\beta) + h_1 Y_{\dot{v}} \tag{2.19}$$

Roll damping. Note that this is the only damping term empirically modeled using this approach, since the other damping related terms are already accounted for in the hydrodynamic force estimate results from interpolation of drift test results.

$$K_p = -(1 - \sin\beta)(.029C_V + .02\lambda)\rho g b^4\sqrt{b/g} + h_1 Y_v \tag{2.20}$$

$k(\beta)$ term is the hull added mass function

$$k(\beta) = .06641 + .00716\beta + .0003861\beta^2 \tag{2.21}$$

h_1 represents the moment lever arm that couples sway to roll

$$h_1 = (vcg - .3927b\tan\beta)(vcg - .306b) \tag{2.22}$$

[71] shows through experiments and analysis that surge added mass is approximated 8% of vessel mass in planing vessels.

These equations allow for a dynamically coupled time-invariant estimation of added mass and roll damping about a steady state trajectory. Judge offers an empirical procedure to

attain time varying estimate of wetted chine length L_C dependent on roll angle [32]. However, for simplicity, we assume that the chine wetted beam is equal to vessel beam and preclude a dry chine condition. This may introduce inaccuracies in large transient roll angles. However, since our primary use in the model is in steady state optimization and control design based on linear stability assessments, treating added mass as a steady time-invariant term about the mean equilibrium provides a low cost solution that is appropriate for our application.

2.2 Establishing 4DOF System

We define state vectors, separate matrices for rigid body centripetal terms, mass, damping, hydrodynamic force, and control forces according to [23]. Experimental data from static capture and rotating drift tests on prismatic hulls of various deadrise from Brown & Klosinski [8] are used in an interpolative fashion as introduced by Katayama [35] to model hydrodynamic forces associated with restoring forces and damping on u, v, p, and r velocities. We use a subset of data, taken at a fixed velocity in the fully planing regime with Froude number 3 to remove surge dynamics and focus our study on aspects related to roll-sway-yaw. Added mass expressions are modeled using [38] and steady state trim is estimated using [55].

Second-order equations of motion are set up as a system of first-order differential equations to simulate trajectories and evaluate maneuvering characteristics. Spring mass damper characterizes the system with mass, roll damping that is not represented by the hydrodynamic forces modeled from the interpolated test data, and Coriolis terms on the left and hydrodynamic forces determined through interpolation of test data and control forces on the right.

$$A\dot{\eta} + B\eta + C_{RB}\eta = F \tag{2.23}$$

$$\eta = \begin{bmatrix} \dot{x} & \dot{y} & \dot{\phi} & \dot{\psi} \end{bmatrix}' = \begin{bmatrix} u & v & p & r \end{bmatrix}' \tag{2.24}$$

$$\dot{\eta} = A^{-1}(-B\eta - C_{RB}\eta + F) \tag{2.25}$$

The mass matrix A in equation 2.27 is in body fixed coordinate system and includes both rigid body and added mass. The terms are developed in section 2.1.2.

$$A = \begin{bmatrix} m_b & 0 & 0 & 0 \\ 0 & m_b & 0 & 0 \\ 0 & 0 & I_{xx} & -I_{xz} \\ 0 & 0 & -I_{xz} & I_{zz} \end{bmatrix} \tag{2.26}$$

$$+ \begin{bmatrix} X_{\dot{u}} & 0 & 0 & 0 \\ 0 & Y_{\dot{v}} & 0 & Y_{\dot{r}} \\ 0 & 0 & K_{\dot{p}} & 0 \\ 0 & N_{\dot{v}} & 0 & N_{\dot{r}} \end{bmatrix} \tag{2.27}$$

The damping matrix B consists of the single roll damping term K_p. It characterizes the damping force that is not captured through interpolation of the drift test data as described in section 2.1.2.

$$B = \begin{bmatrix} 0 & 0 & 0 & 0 \\ 0 & 0 & 0 & 0 \\ 0 & 0 & K_p & 0 \\ 0 & 0 & 0 & 0 \end{bmatrix} \tag{2.28}$$

The Coriolis matrix C_{RB} utilizes reference [23].

$$C_{RB} = \begin{bmatrix} 0 & 0 & 0 & -m_b(x_g r + v) \\ 0 & 0 & -m_b y_g p & -m_b(y_g r - u) \\ 0 & m_b y_g p & 0 & 0 \\ m_b(x_g r + v) & m_b(y_g r - u) & 0 & 0 \end{bmatrix} \tag{2.29}$$

The external forces acting on the system are a sum of the individually modeled forces as categorized into the following vectors: 1) hydrodynamic forces determine through interpolation of drift and rotating test data, 2) hydrodynamic forces induced by the rudder as developed in section 2.2.1 and 3) dynamics associated with AMA inertial mass on the vessel - AMA system as developed in section 2.2.2.

$$F = \begin{bmatrix} [F_{HD}] & [F_{rud}] & [F_{mass}] \end{bmatrix} \tag{2.30}$$

Each vector consists of forces acting in thrust (X), sway (Y), roll (K), and yaw (N).

$$F = \begin{bmatrix} X_{HD} & X_{rud} & X_{mass} \\ Y_{HD} & Y_{rud} & Y_{mass} \\ K_{HD} & K_{rud} & K_{mass} \\ N_{HD} & N_{rud} & N_{mass} \end{bmatrix} \tag{2.31}$$

The 2nd order system is then established as a system of 1st order differential equations to facilitate numerical integration. Forces are summed in each row over columns comprising of hydrodynamic and relevant rudder and/or inertial mass induced forces. The rotation matrix provides the ability to track position in inertial reference frame while remaining states are accounted for in body reference frame with the origin at the center of mass

$$\nu = \begin{bmatrix} x & y & \phi & \psi & u & v & p & r \end{bmatrix}' \tag{2.32}$$

$$\dot{\nu} = \begin{bmatrix} 0 & R \\ 0 & -A^{-1}B \end{bmatrix} \nu + \begin{bmatrix} 0 & 0 \\ 0 & -A^{-1}C_{RB} \end{bmatrix} \nu + \begin{bmatrix} 0 \\ \Sigma A^{-1}F \end{bmatrix} \tag{2.33}$$

$$R = \begin{bmatrix} cos(\psi) & -sin(\psi) & 0 & 0 \\ sin(\psi) & cos(\psi) & 0 & 0 \\ 0 & 0 & 1 & 0 \\ 0 & 0 & 0 & 1 \end{bmatrix} \tag{2.34}$$

2.2.1 Rudder to Vessel Dynamics in 4DOF

Rudder dynamics affect forces on all four degrees of freedom. Experimental data shows that parameters affecting the rudder can be decoupled from those affecting the hull. Maneuvering forces of sway and yaw on the hull are highly dependent on deadrise, trim and heel angles since they establish the angle of attack of hull lifting surfaces. However, changes in deadrise have little effect on rudder induced maneuvering forces of sway and yaw in analysis of [8]. Because of the relation of deadrise with heel and trim are inextricably linked, we can conclude that forces induced by the rudder would also be relatively unaffected by heel and trim. Thus, we model rudder forces as decoupled from the vessel hull attitude parameters and only dependent on rudder angle of incidence.

Induced translational forces of X and Y are best fit to rudder angle of deflection and angle of incidence as determine by forward and sway velocities. We take advantage of the results of Sugai [58] as referenced in [38] that show turning diameter as not strongly dependent on rudder geometry as long as the rudder planform is greater than 1/30 of the product of the static draft and water length. This simplification eliminates model dependency on rudder specific geometries and reduces computation cost. Our proposed model based on classic wing theory is simplified and dependent only on forward velocity, input angle and drift angle, enabling low-cost accuracy. It is then best fit to experimental data.

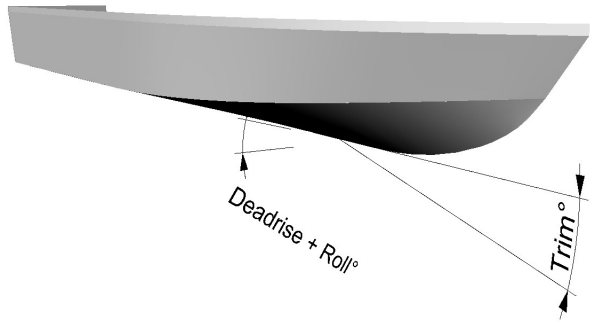

Figure 2.3: Attitude Parameters: Changes in deadrise affect the angle of incidence of the vessel with oncoming fluid. While the hydrodynamic forces on the hull are highly dependent on these angles of incidence, forces acting on the rudder are relatively unaffected as shown in experimental data [8]

Rudder dynamics are modeled using classic wing theory and fit to data independent of vessel attitude parameters. δ represents rudder angle from centerline, α the angle of attack of the rudder with oncoming fluid, and u forward velocity.

$$X_R = \frac{1}{2}\left(A_D\delta^2 + B_D\delta + C_D\right)u^2 \tag{2.35}$$

$$Y_R = \frac{1}{2}A_L u^2 \alpha cos\left(\delta\right) \tag{2.36}$$

$$K_R = Y_R vcg \tag{2.37}$$

Roll moment is the multiple of sway force with distance from center of force application on the rudder to the vertical center of gravity, vcg.

$$N_R = Y_R lcg \tag{2.38}$$

Similarly, the yaw moment is the multiple of rudder induced sway force with distance from rudder to the longitudinal center of gravity, lcg.

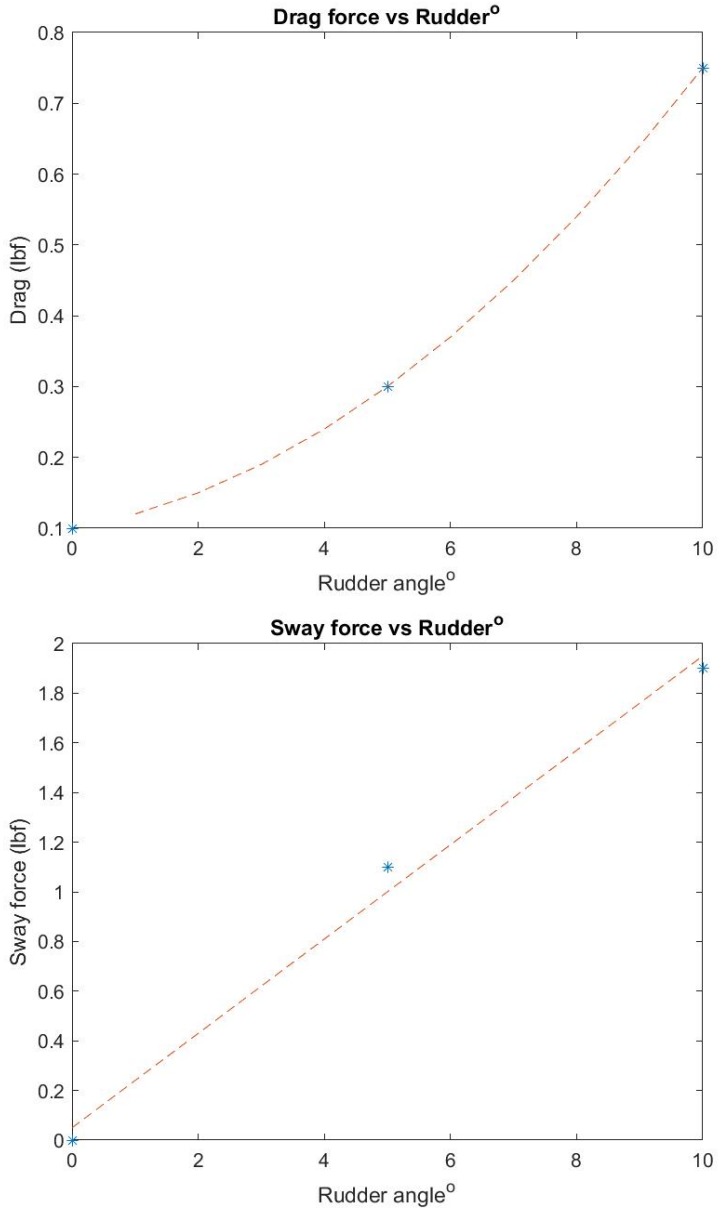

Figure 2.4: Rudder Model ID: Experimental rudder data from [8] in drag and sway for both 10° and 20° deadrise in wind axes without air tare are approximately equal, showing little sensitivity to deadrise. Data is fit to a second order and linear model respectively

	Fit values
A_D	4.6 e -5
B_D	1.38 e -4
C_D	9.2 e -4
A_L	1.8 e -3

Hydrodynamic forces induced by the rudder are characterized by these empirical equations and expressed in equation 2.39 for use in equation 2.33

$$F_{rud} = \begin{bmatrix} X_{rud} & Y_{rud} & K_{rud} & N_{rud} \end{bmatrix}' \tag{2.39}$$

The inertial effects of a moving rudder on the vessel on yaw axis are considered negligible compared to the inertial effects of a lateral moving AMA on the roll axis. For our example vessel, we can see that by applying the parallel axis theorem on I_{zz} to the point of rudder moment application, considering the rudder inertia's effect on the vessel is over 80 times smaller than the effect of the AMA's inertia on the vessel's roll motion. For simplicity, rudder inertia is neglected and rudder input is established in the angle deviation from center. With the AMA in fixed position, the vessel - rudder system is considered in 4DOF. The set of these equations 2.35, 2.36, 2.37, 2.38, are then used in equation 2.31. Next, we consider the effects of an inertial mass in a non-centered position on the vessel.

2.2.2 Mass Actuator Dynamics - 4DOF

In a 4DOF vessel model, the AMA is fixed to the vessel and an off-center position induces a roll moment with the distance from center essentially acting as a lever arm. m_a represents the

weight of the inertial mass. For the demonstration purposes of this paper, this is equivalent to 10% of vessel mass. d is the lateral distance from mass to vessel centerline. Equation 2.40 is used in equation 2.31. K_{mass} of equation 2.40 represents the roll moment induced by AMA on the vessel-AMA system in 4DOF. Since the AMA only induces moment about roll, K_{mass} is the only non-zero term in F_{mass} used on equation 2.33.

$$K_{mass} = m_a g d cos(\phi) \tag{2.40}$$

$$F_{mass} = \begin{bmatrix} 0 & 0 & K_{mass} & 0 \end{bmatrix}' \tag{2.41}$$

Next, we consider the effects of this inertial mass free to move.

2.3 Establishing 5DOF System

An AMA free to move on the vessel's lateral axis has dynamics that necessitate the integration of a fifth degree of freedom. These dynamics can be obtained through expressions of kinetic and potential energies and a Lagrangian approach. The vessel - free AMA model becomes 5DOF system.

The AMA's dynamics in body reference frame act in 2DOF on roll (ϕ) and actuator mass position from centerline (d), which we use Lagrange's method given in [eq: 2.42] to mathematically describe.

$$\frac{d}{dt}(\frac{\partial T}{\partial \dot{q_i}}) - \frac{\partial T}{\partial q_i} + \frac{\partial U}{\partial q_i} = F_i \tag{2.42}$$

Kinetic and potential energies are expressed as:

$$T = \frac{1}{2} I_x \dot{\phi}^2 + \frac{1}{2} m_a [(d\dot{\phi})^2 + (z_o \dot{\phi} + \dot{d})^2] \tag{2.43}$$

$$U = m_a g z_o \, (cos\phi - 1) - m_a g d sin\phi \tag{2.44}$$

z_0 represents the vertical distance the inertial mass is positioned above the vertical center of gravity. I_x is the vessel's overall moment of inertia about the roll axis. Substituting [eq: 2.43] and [eq: 2.44] into [eq: 2.42] and differentiating with respect to d and ϕ yields [eq: 2.45] and [eq: 2.46]:

$$\frac{d}{dt}[(m_a(z_o\dot{\phi} + \dot{d})] - m_a d\dot{\phi}^2 - m_a g sin\phi = F_d \tag{2.45}$$

$$\begin{aligned} &\frac{d}{dt}[I_x\dot{\phi} + m_a(d^2\dot{\phi} + z_o(z_o\dot{\phi} + \dot{d})] \\ &\qquad - m_a g z_o sin\phi - m_a g d cos\phi = F_\phi = -z_o F_d \end{aligned} \tag{2.46}$$

Solving these equations and rearranging terms, we attain a new expression for the roll force that the AMA exerts on the vessel within the structure of [eq. 2.25]. F_d is the force the actuator exerts on the control mass. This expression is used instead of [eq. 2.40] in our 5DOF model.

$$K_{mass} = m_a(gdcos(\phi) - 2d\dot{d}\dot{\phi} - z_o d\dot{\phi}^2) - z_0 F_d \tag{2.47}$$

Just as in the 4DOF system, AMA is not coupled with other forces in the vessel's surge, sway, or yaw directions and remains the only term in F_{mass} in equation 2.41.

In characterizing the AMA's motion in body reference frame, Eq. [2.48] establishes a fifth degree of freedom of the AMA free to move laterally within the vessel.

$$\ddot{d} = d\dot{\phi}^2 + gsin(\phi) - z_0\ddot{\phi} + \frac{F_d}{m_a} \tag{2.48}$$

The vessel and control mass system moment of inertia about the roll axis becomes a state dependent variable in the 5DOF model.

$$I_{xx} = I_x + (d^2 + z_o^2)m_a \tag{2.49}$$

Establishing 5DOF equations of motion using these dynamics, we use the same approach as we did with the 4DOF equations. d represents the inertial mass position from center in body reference coordinate frame, F_d the active actuation force applied on the AMA inertial mass. We establish sub-blocks to account for its dynamics and second order equations are expressed in the system of single order differential equations.

$$M = \begin{bmatrix} 1 & 0 \end{bmatrix}' \tag{2.50}$$

$$F_{AMA} = \begin{bmatrix} 0 & F_d \end{bmatrix}' \tag{2.51}$$

$$\nu_5 = \begin{bmatrix} \nu_4 & d & \dot{d} \end{bmatrix}' = \begin{bmatrix} x & y & \phi & \psi & u & v & p & r & d & \dot{d} \end{bmatrix}' \tag{2.52}$$

$$\dot{\nu} = \begin{bmatrix} 0 & R & 0 \\ 0 & -A^{-1}B & 0 \\ 0 & 0 & M \end{bmatrix} \nu + \begin{bmatrix} 0 & 0 & 0 \\ 0 & -A^{-1}C_{RB} & 0 \\ 0 & 0 & 0 \end{bmatrix} \nu + \begin{bmatrix} 0 \\ \Sigma A^{-1}F \\ m_a^{-1}F_{AMA} \end{bmatrix} \tag{2.53}$$

Equation 2.53 represents the nonlinear equations of motion of the 5DOF system including a rudder dynamics and an inertial mass free to move laterally within the vessel. These dynamics as written in MATLAB code are shown in Appendix C with a link to a GITHUB repository in Appendix A

Chapter 3

COUPLED PLANING DYNAMICS

Empirical methods to date have not adequately characterized roll yaw coupling, which is an essential dynamic in characterizing the effects of asymmetrical mass distribution. Goal for this section: provide analysis for this dynamic.

Yaw moment expressions offered by (E. Lewandowski, 2004) lack roll dependency which is evident in the B&K test data as shown in Appendix B. Two-dimensional methods do not provide a direct method to evaluate the three-dimensional problem of roll yaw coupling. It is only able to directly evaluate the 2D effects of sway, heave, and roll, but requires the integration of the 2D sectional sway forces to attain a 3D model for yaw moment. It lacks an explicit expression for the location of the sway center of pressure which is fundamental factor to sway yaw coupling. 2D+t methods are unable to provide direct evaluation that is offered by an interpolative method.

Test data first allows analysis of sway force (Y) behavior sensitivities to roll and crossflow. With measurements of sway force (Y) and yaw moment (N), we can analyze the model for the lever arm that couples Y to N. Finally, we provide analysis for general yaw moment (N) behavior.

3.1 Sway Force Center of Pressure

[38] described the yaw moment as the product of sway force and a lever arm between the longitudinal centers of hydrodynamic pressure (Cp) and center of gravity (LCG). Thus, the coupling between sway force and yaw moment can be modeled as the lever arm between the sway force center of pressure (Cp) and longitudinal center of gravity (LCG). In the Brown & Klosinski [8] captive tow tank tests, the yaw moment measurement was taken at the tow

point located 22.5 inches forward of the transom. In order to evaluate the lever arm, we first adjust the yaw moment as measured in the captive tank tests to an estimated center of gravity for a free body model. This involves calculating the the steady state free body center of gravity using a force balance with Savitsky method with the running trim angle. Then, a lever arm model can then be obtained through interpolation of available sway force and yaw moment data.

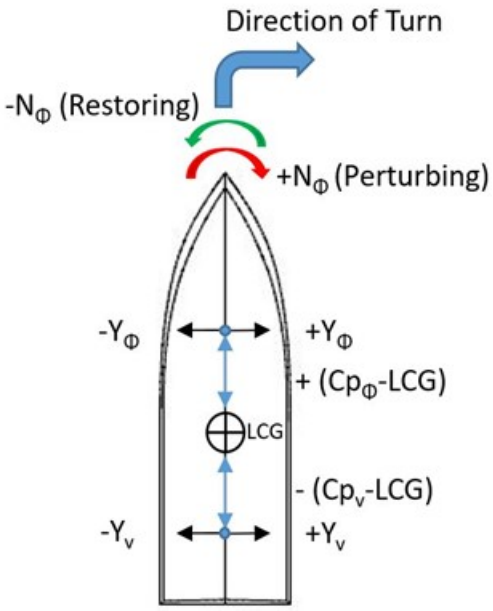

Figure 3.1: Yaw Coupling: The distance between center of force (Cp) and longitundinal center of gravity (LCG) acts as the moment arm that translates sway force to yaw moment (N)

$$C_p - LCG = \frac{N}{Y} \tag{3.1}$$

By plotting the resultant model, we can further evaluate of Cp for Y_ϕ and Y_v contributions. Analysis of plots show a general trend that sway force due to roll (Y_ϕ) acts forward of LCG,

where sway force due to crossflow (Y_v) acts aft of LCG. This is most clearly demonstrated in at low deadrise (10°) and low trim (3°). The corresponding steady state LCG is approximately 1.5 ft from transom. Data on lever arm distance is plotted against roll angle and side slip angle and interpolated with thin plate spline method. With no cross flow, sway force acts forward of LCG and moves further forward with increasing roll angle. Crossflow, as manifested in positive non-zero side slip angle, moves the center of pressure aft. A similar trend is exhibited when trim is brought up to 6° by shifting LCG aft to 0.8 ft from transom. Similar general behavior observe in both trim conditions with 10° deadrises with a positive Y_ϕ forward of LCG and Y_v that acts aft of LCG.

Yaw moment divided by sway yields the distance between center of longitudinal pressure and lcg (Cp-LCG) which couples sway to yaw. The results of (Brown & Klosinski, 1994) are adjusted to model a free body vessel with steady state trim angle in force balance as a function of lcg as calculated using Savitsky methods. Cp-LCG is shown near the ends of the range of our analysis, at 10° and 20° deadrise, and trim at 3° and 6°, noting that this analysis holds less value near the origin since N/Y presents a singularity. Away from the origin, the data shows clear dependencies of Cp-LCG on trim, deadrise, roll angle, and sway. These relations are difficult to describe empirically, but relatively inexpensive to numerically assess through interpolation.

An analysis of these manifolds indicates a consistent behavioral trend. The increase in cross flow as represented by crossflow angle β induces an aft movement of yaw lever arm (Cp-LCG) that couples sway to yaw; increasing sway acts further aft on the vessel countering the yaw moment of a turn. This observation corroborates the findings of a number of previous studies by Faltinsen (1990), Beukelman and Journee (2001) or Golding et al. (2006) [52] [26] that indicate the cross-flow drag as a function solely of the fluid velocity athwartship. This provides positive indication on the validity of our data and approach.

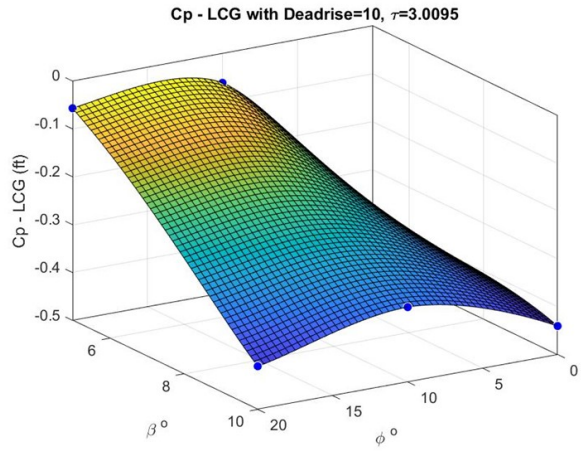

(a) Low deadrise, low trim

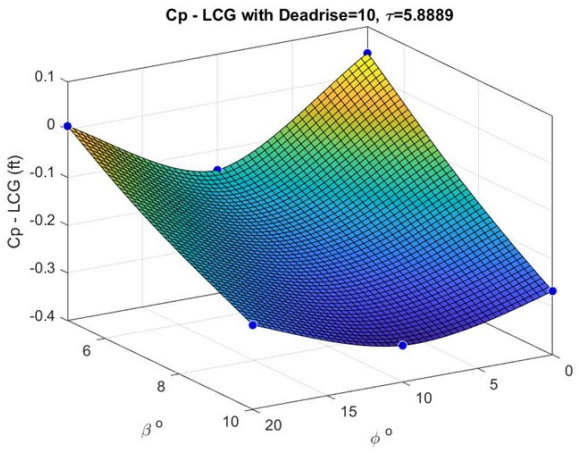

(b) Low deadrise, high trim

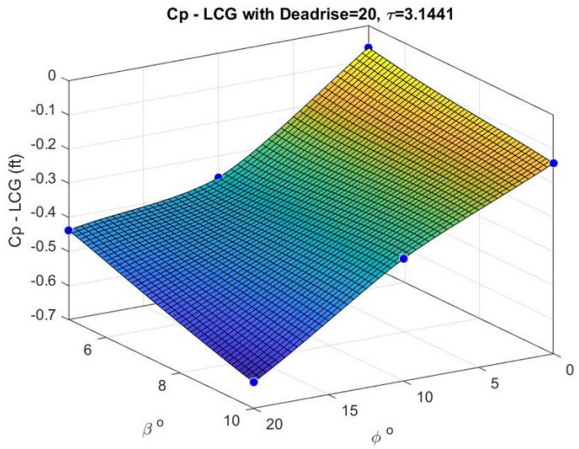

(c) High deadrise, low trim

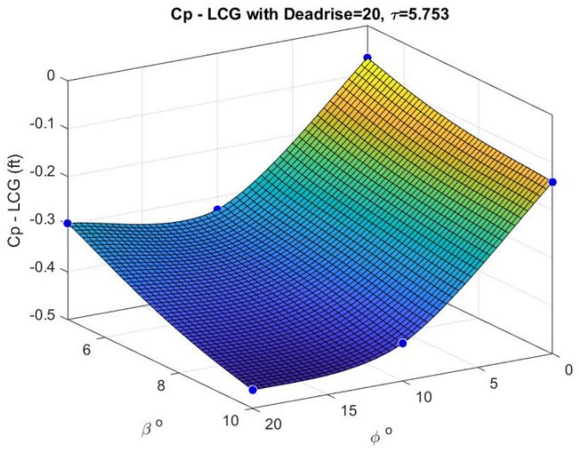

(d) High deadrise, high trim

Figure 3.2: Cp-LCG(β,ϕ): demonstrates the moment arm that couples sway to yaw dependencies on sway velocity as represented by crossflow angle β and roll angle. Figures show that increasing crossflow moves the center of application aft resulting in yaw moment that counters direction of turn

3.2 Roll to Yaw Coupling

Heel induced yaw moment is not well explored in literature but would be an essential mechanism for maneuver of vessels without an aft steering mechanism such as a rudder. [7], [17] observed that heel can induce yaw both for and against the direction of heel depending on unspecified conditions, which can be directly assessed with our linearized system model. The term $\widetilde{A_{83}}$ of the linearized matrix that directly couples heel ϕ to $\dot{r}$ provides this information. A positive value indicates $+N_\phi$ where heel induces yaw moment in the same direction, while a negative value $-N_\phi$ represents the opposite.

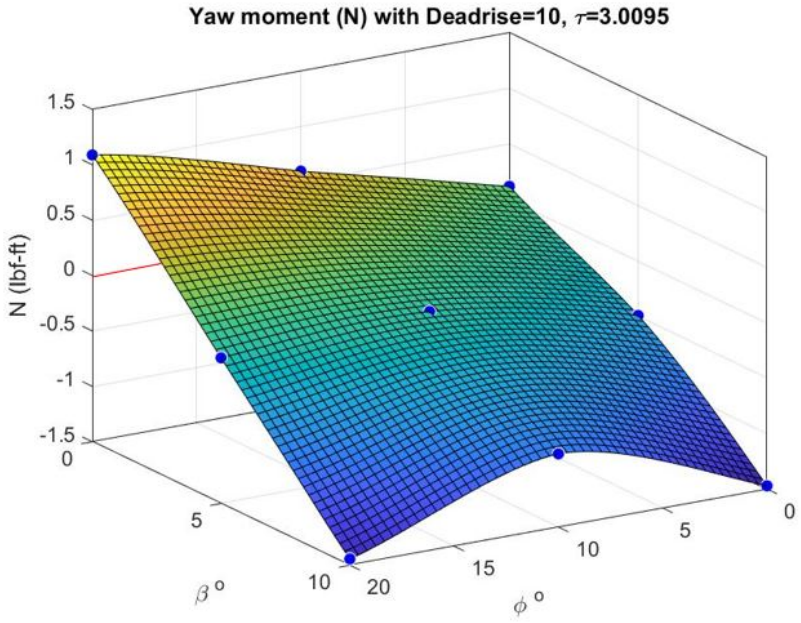

Figure 3.3: $+N_\phi$: Positive manifold represents roll induced yaw force in the direction of roll and desired behavior for turning without a rudder, which occurs at low deadrise

As observed in the experiments from (Brown & Klosinski, 1994), induced yaw moment at lower 10° deadrise angle is generally in the same direction as heel ($+N_\phi$) and the opposite ($-N_\phi$) at higher 20° deadrise. For a vessel to turn to be supported by roll to yaw coupling and without the aid of a rudder, we require a low deadrise condition due to the associated

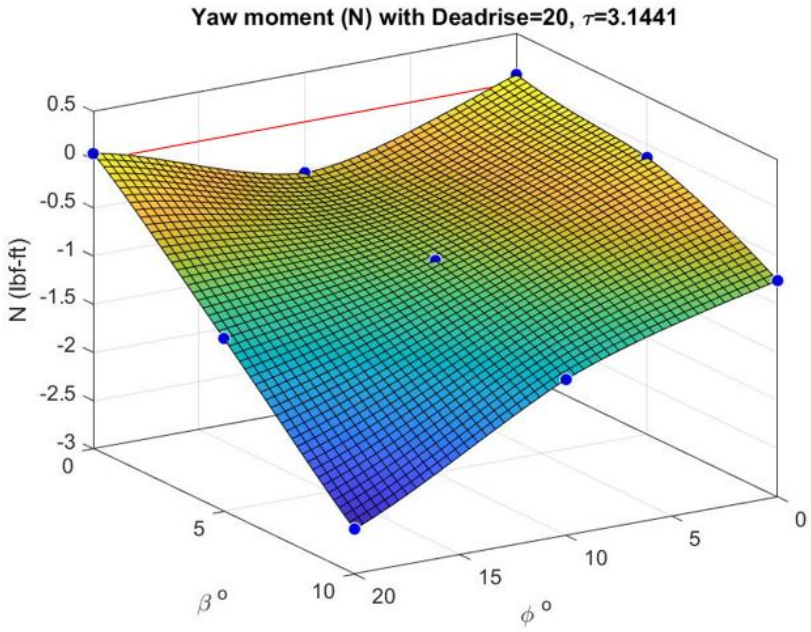

Figure 3.4: $-N_\phi$: Negative manifold represents roll induced yaw force opposite the direction of roll and non-desired behavior for turning without a rudder, which occurs at high deadrise

$+N_\phi$ dynamic. This will be simulated in the following chapter.

Plots of Figure 3.5 show yaw moment shown as a function of roll, sway, deadrise, and trim across our data range. As expected from the results of 3.2, there is the near linear relation (shown in red arrow) between yaw moment and sway. In all conditions, increasing sway yields increasing restoring moment. As a vessel enters a turn, sway force and corresponding yaw restoring moment increases until the vessel reaches steady state equilibrium where restoring yaw moment equals in magnitude to the perturbing moment presented by the steering mechanism. This matches our intuitive understand of turning dynamics.

In addition, figure 3.5 show trim dependent behavior that has practical implications on vessel loading. Low trim results in higher coupled effects between crossflow and roll. Let us consider a realistic scenario of a steady state turning trajectory with a rudder and the effects of shifting weight fore or aft during that turn. Initially, forces are in balance between a perturbing yaw moment of a steering mechanism and crossflow induced restoring moment. If

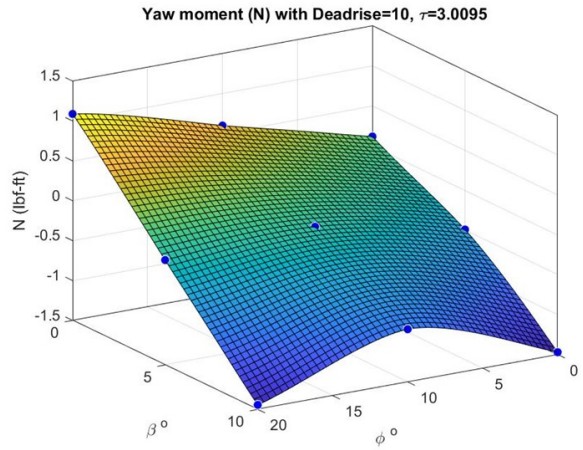

(a) Low deadrise, low trim

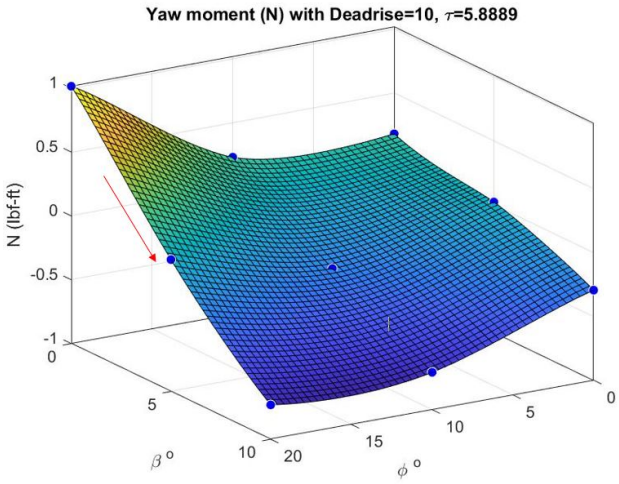

(b) Low deadrise, high trim

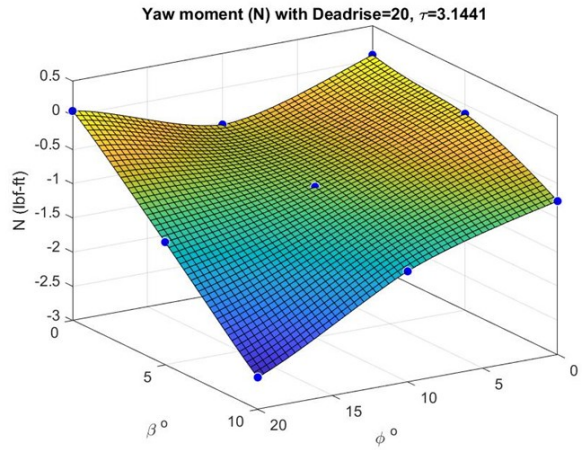

(c) High deadrise, low trim

(d) High deadrise, high trim

Figure 3.5: N(β,ϕ): yaw moment as a function of sway velocity as represented by crossflow angle β and roll angle.

weight was suddenly moved aft, it would increase the trim and place the vessel on a manifold of reduced restoring moment. Since the perturbing moment from the steering mechanism remains constant, the net effect would be yaw acceleration and a sharper turn. In the context of a low deadrise vessel without a rudder, higher roll to yaw coupling is desired and moving weight forward would result in higher effectiveness.

Coupled dynamics as shown through interpolation of planing test data have large potential to be exploited for optimization and trajectory planning using methods developed for similar applications. Sakaki [53] uses genetic algorithms to determine optimal trim and interceptor design. Ayob [4] optimizes based on calm water resistance and steady turning diameter using basic empirical turning equation 4.1. Masumi [42] uses drag and porpoising stability as considerations to optimize aspect ratio, LCG and deadrise parameters. Castro-Feliciano's [12] [13] work in co-design of planing vessels optimizes vessel geometric parameters with control architecture resulting in improved performance in comparison to a traditional sequential design process. These approaches would work well with our model and would be an ideal subject for follow on development.

Chapter 4

TIME DOMAIN SIMULATION METHODS

For an initial assessment, we simulate turns to starboard on models of both 10° and 20° deadrise and compare the results to previous models and experiments of planing hulls maneuvering with an aft steering mechanism or rudder. In this section, we will assess computation time, steady turning diameters, advances, tactical diameters, drag resistance, and maneuver effects of heel. Rudder input is set at -5° (turn to starboard) with lcg at 1.2 ft from transom corresponding to trim angles of 4.1 and 4.8 respectively. Equations of motions were integrated using various methods for comparison; though all showed similar accuracy, the MATLAB implicit variable order integration function ODE15s performed significantly faster. Trajectories are plotted on x-y and states against time. Model vessel dimensions and characteristics mirror those used in the tests of [8], [9] and are summarized here for convenience. Certain parameters that had minimal variability were assumed constant.

b Beam length: 9 in

m_b Vessel mass: 11.49 lbs

m_a Control mass: 0.1 m_b

loa Length overall: 50 in

vcg Vertical center of gravity: 0.25 ft (unless otherwise mentioned)

lk Wetted keel length: 1.95 b

z_0 Distance of control mass above vcg: 0.1 ft

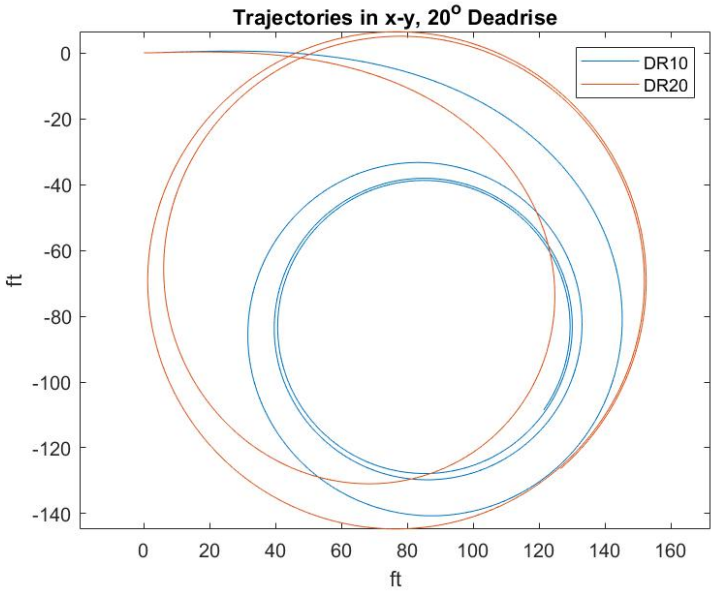

Figure 4.1: X-Y Plots: show the differences in Advance, Tactical Diameter, and Steady Turning Diameters are shown in the time domain trajectories of simulations between with vessels of 10° and 20° deadrise

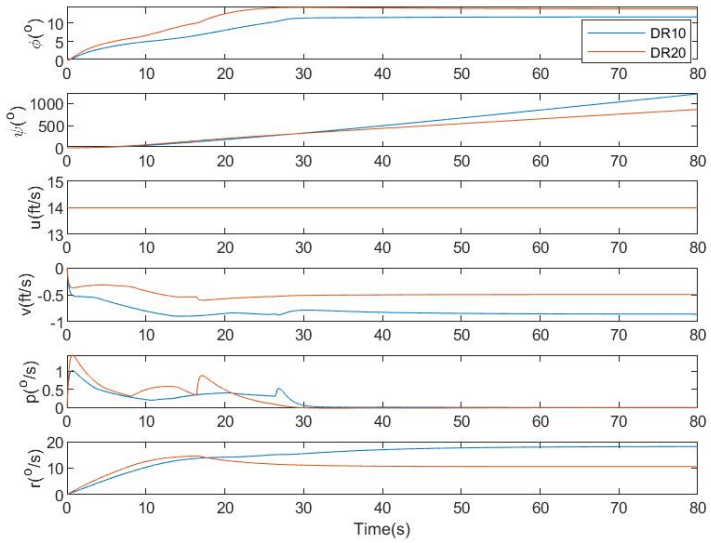

Figure 4.2: Time Domain Simulation: rudder actuated turns with 10° vs 20° deadrise. Rudder angle of -5°, vcg of 0.25 ft, lcg of 1.2 ft from transom, and at fixed forward velocity with Froude number of 3.

Method	Resource	Time required
CFD (Star CCM)	20 core parallel	323 hrs
2D+t (MATLAB)	i7-4510U	2 hrs
Our method (MATLAB)	i5-8250U	11 seconds

Table 4.1: Computation resource comparison between modeling methods

4.1 Computational Cost

These simulations took an average of 11 seconds to perform 80 second simulations on a standard laptop running an Intel i5-8250U processor without optimization considerations, such as use of parallel processing routines. A comparison to computational requirements for similar simulations using other techniques by Algarin & Bula [2] are provided in Table 1. Though not identical simulation problems, they may serve as rough order of magnitude representatives for comparison.

Our proposed method of interpolation based modeling requires significantly lower cost. Intuitively, we can reason that instead of performing potential flow calculations on a large number of vessel cross sections and integrating for overall vessel dynamics, our model only needs to perform a interpolation based on pre-loaded tables. Requiring 0.14 seconds in computation time for every simulated second, our model simulates faster than real time and may prove particular usefulness in control applications such as Model Predictive Control (MPC). The simplifications employed allow impressive speed. These simplifications include holding heave and pitch constant, using time-invariant expressions for added mass about the mean trajectory and empirical equations to model rudder force independent of rudder geometry or vessel attitude parameters as described in section 2.2. Though the model is impressively faster, note that it is built for the express purpose to offer only an initial evaluation of the maneuver dynamics of a planing hull with a focus on roll-yaw coupled dynamics. For this intended purpose, the low-cost offers an attractive feature as an initial

design tool.

To verify that the numerical integration scheme was not dramatically altering the results, a stiffer problem was presented and a variety of MATLAB methods were compared. Conditions were selected to yield a marginally stable oscillatory response and the trajectory was simulated to 200 seconds.

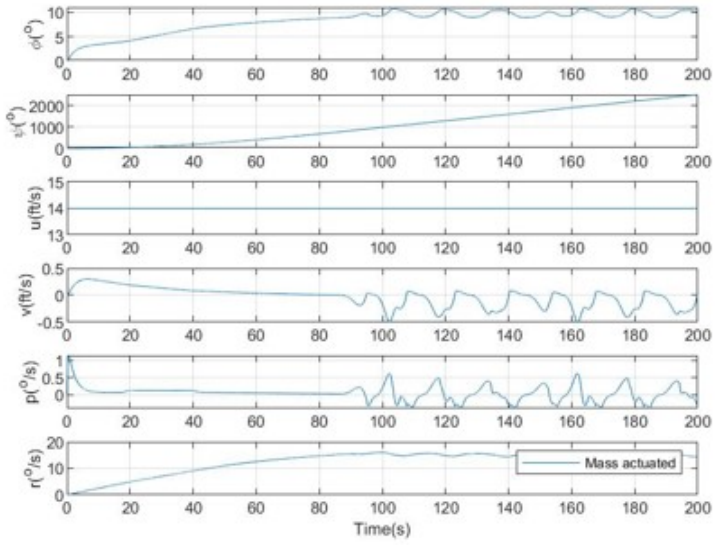

Figure 4.3: Time Domain Response of a Marginally Stable Trajectory: Given straight path initial conditions, the trajectory develops into a bounded oscillations

Integration method	Processing (200s sim)	Final X-Y
ODE15s	93 s	173.3, 143.4
ODE23s	381 s	172.0, 143.0
ODE23	121 s	172.5, 143.1
ODE45	158 s	172.5, 143.0

Table 4.2: Model performance is significantly better using an implicit integrator

Note that the final X-Y position calculated for all trajectories after 200 seconds of simulated travel differ by less than 6 inches, providing reasonable confidence that our method provides consistent results independent of the numerical integration method. Because model performance is best with the ODE15s implicit integrator, this will be the chosen method for the remainder of the simulations within this study.

4.2 Comparison of Turning Metrics

With a model that is able to simulate planing maneuvers, we are able to compare simulated results with other test results other than [8]. Relevant metrics found include Standard Turning Diameter (STD), Advance (Ad), Tactical Diameter (TD), ratio of initial drag resistance to steady turning resistance (R0/RT), and yaw rate dependency on vcg.

4.2.1 Steady Turning Diameters (STD)

The difference in simulated maneuver trajectories reflect the sensitivity of the hydrodynamics of planing vessels' hulls to attitude parameters of deadrise, trim and heel. We compare these results to an empirical maneuvering model based on (Denny & Hubble, 1991) and later simplified by (E. Lewandowski, 2004) which is agnostic of vessel attitude parameters.

$$\frac{STD}{loa} = \left(1.7 + .0222 F_{\nabla} \left(\frac{L}{\nabla^{1/3}}\right)^{2.85}\right) \frac{30}{\delta} \tag{4.1}$$

Note the dependency of this model on displacement as represented by $\frac{L}{\nabla^{1/3}}$. Using a value of 4 and comparing turning diameter:

The models are reasonably close though our current method provides valuable insight on the sensitivity of maneuver to attitude parameters of trim, heel, and deadrise. Next, we run multiple simulations across our model range.

Current Model 10° DR	Current Model 20° DR	Denny & Hubble / Lewandowski
89	151	142

Table 4.3: Comparison of steady turning diameter of our simulation with previous empirical model

Deadrise°	Trim°	Heel°	Rud°	Ad	TD	AdTD	SS R	R0/RT	V0/VT
10	3	3.54	5	149.9	161.2	0.93	60.68	0.754	0.868
10	6	12.16	5	183.5	165.5	1.1	37.6	0.735	0.858
20	3	8.22	5	123.9	146.1	0.848	60	0.951	0.975
20	6	9.27	5	203.9	217.7	0.967	67.2	0.955	0.977
10	3	15.55	10	108.8	107.6	1.01	28.95	0.651	0.807
10	6	19.31	10	150.57	122.36	1.23	25.55	0.552	0.743
20	6	18.87	10	156.61	151.6	1.0331	40.53	0.709	0.842

Table 4.4: Results of simulation with trajectory parameters varied across the model range. Lcg is varied to achieve trim angles between 3° to 6°. Ad - Advance, TD - Tactical Diameter, AdTD - Advance to Tactical Diameter ratio, SSR - Steady Radius, R0/RT - Initial drag resistance to steady drag during turn with velocity held constant, V0/VT - initial velocity to steady turn velocity with thrust held constant

4.2.2 Advance to Tactical Diameter

A meaningful metric is a ratio of advance (Ad) to Tactical Diameter (TD). Larger advances represent longer transient phases before reaching steady yaw rates. Experimental data has shown that the more drastic the turn, the larger the advance in comparison with tactical diameter as shown by Kim & Kim [36]. Gradual turns show a convergence of Ad/TD to unity. To compare our model with previous data, we perform a series of simulations varying deadrise, trim, and rudder inputs, plotting Ad/TD.

These results are consistent with experimental data as conducted in NIWA 1972 tests and referenced in [36]. Note, our simulations have longer TD since velocities are held constant and turns are less drastic to stay within model bounds; nevertheless the Ad/TD ratio and trends are consistent with experimental results.

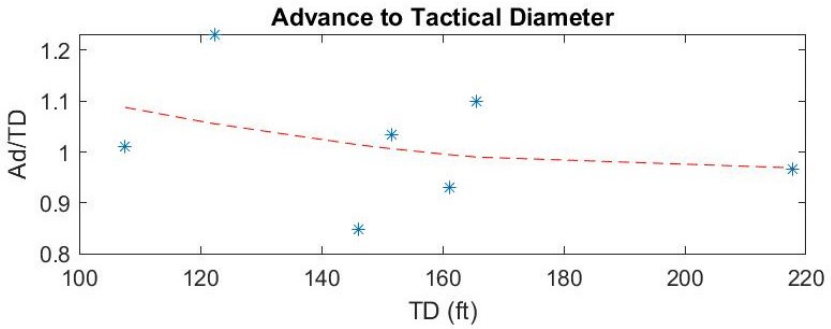

Figure 4.4: Ad/TD: Larger transient as signified by Ad/TD with sharper turns. Blue data points indicate simulated results as shown in Table 4.4 where red dashed trendline represents previous test data

4.2.3 Resistance Trends

Experimental data shows reduction in velocity as a function of turning diameter expressed a ratio of initial velocity prior to the turn to that during steady turn. To model this using our fixed velocity simulation, we model the power required to maintain that constant velocity and use that to estimate a velocity drop if thrust was held constant. The more drastic

the turn as represented by lower tactical diameters, the larger the difference becomes in resistance. At high tactical diameters, the ratio of power required approaches unity. This is also consistent with the NIWA 1972 results though it is shown in Kim & Kim [36] through velocity measurements.

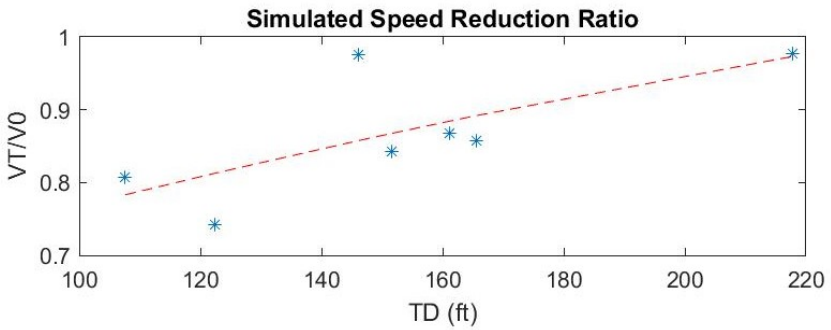

Figure 4.5: Speed Reduction Ratio: Larger speed reduction with sharper turns. Blue data points indicate simulated results as shown in Table 4.4 where red dashed trendline represents previous test data

4.2.4 Yaw sensitivity to vcg and heel

Deadrise and trim have significant role in roll and yaw forces. This is shown in the variations of steady state heel angle and turning diameters modeled through simulation. Our ability to model these effects allows evaluation of methods of control that involve heel.

Deakin [17] tests on generic planing vessel of different vcg. To simulate test conditions, we use a model of deadrise 20° with a lcg of 1.2 ft corresponding to a steady state trim of 5°, and run with vcg of 0.12 and 0.7 ft. Turning maneuvers were conducted up to 5° rudder angle to assess the linear response. Experimental results confirm model simulations in increased outboard heel with higher vcg. Heel angles of 8.92° and 19.97° correspond with low and high vcgs respectively. Note that vessel particulars such as deadrise and geometries were not provided in Deakin [17]. Nevertheless, our model results show a matching trend of higher yaw rate and heel at higher vcg. Dynamically, this indicates that higher vcg increases both

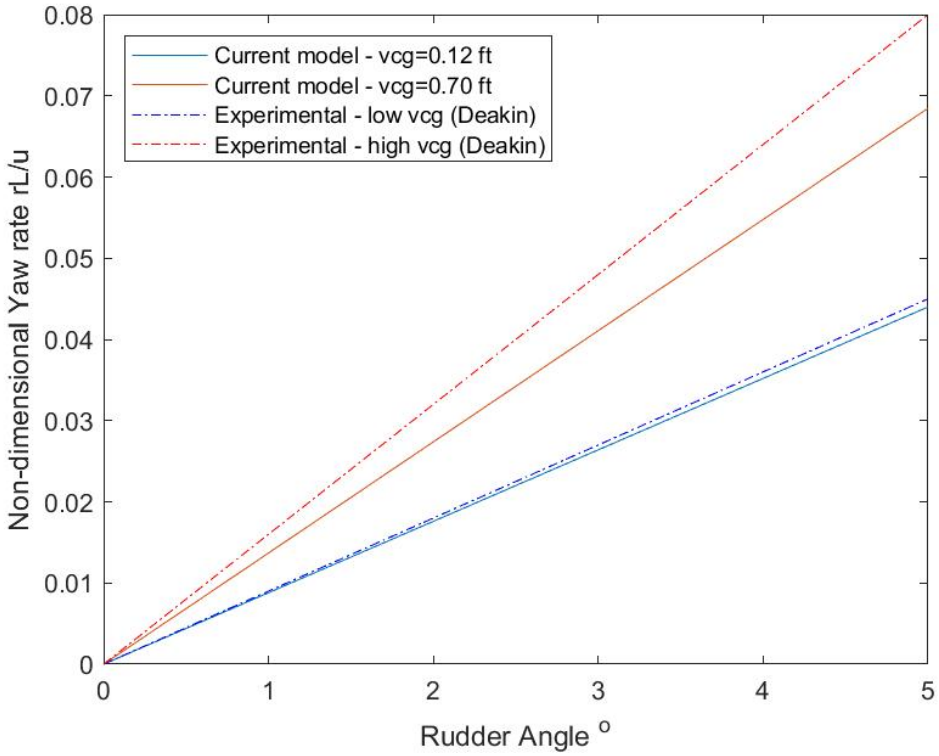

Figure 4.6: Vertical Center of Gravity Influence: model simulation compared with experimental data by Deakin [17])

rudder induced heel and heel induced yaw moment. These results provide positive indication of model fidelity and enables evaluation of asymmetrically loaded vessels.

4.3 Conclusions

A new blended method, relying on interpolation of static drift tests are lower cost, have larger range of applicability, and provides a better understanding of lesser explored dynamics such as roll to yaw coupling. This allows us the ability to consider geometric design parameters for optimization, such as deadrise, simultaneously with controller design. The computation speed of the model is faster than real time, important for control applications such as MPC. Finally, it allows us expedient ways to evaluate the feasibility of non-tradition maneuvering

methods such as using active mass distribution.

Chapter 5

TIME DOMAIN TRAJECTORY SIMULATION

Using our established model, we proceed to simulate trajectories that would be difficult to perform using other means. The aim is to assess stability and maneuvering characteristics of asymmetrical mass distribution on prismatic planing vessel. In this chapter, three types of vessel trajectories are considered. First, we evaluate asymmetrical mass distributions on a 10° and 20° deadrise vessels. Next, we offer analysis on stability of the linearized systems and a comparison of steady drag during turns to demonstrate the potential for optimization. Finally, we simulate a non-oscillatory yaw instability called an "end-swap" spinout, a condition that may be caused by high roll and sway conditions and motivates the development of active control feedback pursued in Chapter 6.

5.1 10° Deadrise

Given positive N_ϕ dynamic on low deadrise vessels, we explore the possibility of using the heel caused by an asymmetrical mass to induce yawing maneuver. Consider a rudderless vessel of 10° deadrise with a mass of 10% of vessel weight placed at its starboard beam. Model simulations show the vessel entering a stable turning trajectory to starboard due to heel induced yaw moment in the direction of heel. Let us also consider an identically hulled vessel but equipped with a rudder and center of mass amidship. Rudder input is set to match the steady turning trajectory of the mass actuated model; both trajectories are plotted against each other for comparison.

With matched steady turning diameters and the transient responses compared, the rudder actuated model exhibits a 23% shorter advance. As shown in the equations of motion, the rudder offers a direct yaw moment application and mass actuation does not. Instead, mass

Model	Um (ft)	Ur (°)	r (°/s)
Rudder	0	-3.035	12.79
Mass	0.3	0	12.79

Table 5.1: Control inputs resulting in the same steady turning rate of a model vessel of 10° deadrise

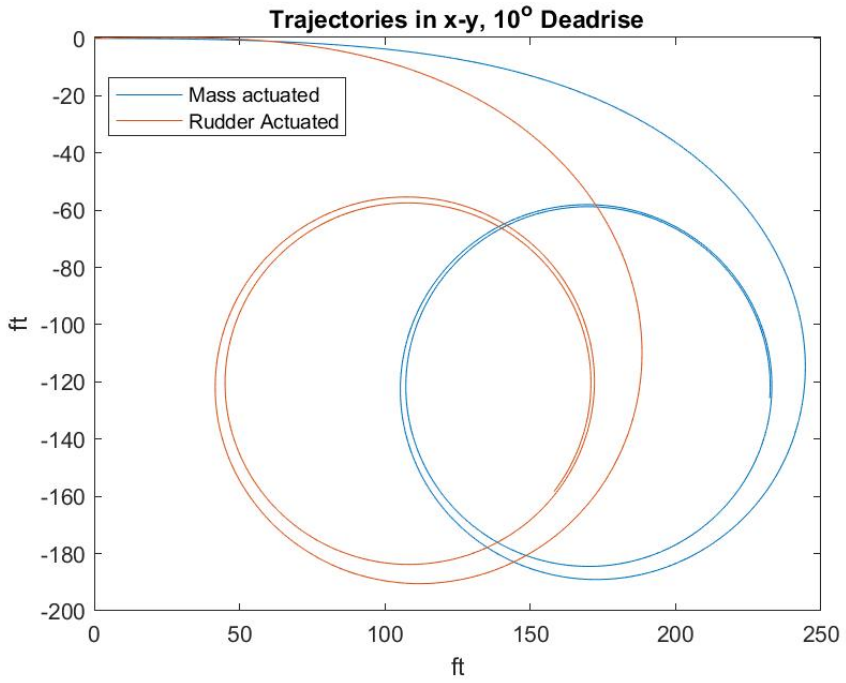

actuation primarily affects roll moment and induces yaw moment from heel to yaw coupling, resulting in a longer advance. This highlights a limitation of the mass actuation method; though the model shows it to be possible, performance is limited by actuator saturation. Unlike a surfer whose body mass may be equal or more than that of the vessel, an internal mass such as a lithium battery aboard as ASV is limited realistically to a fraction of vessel weight with actuation distance confined internal to the vessel hull.

Stability of each vessel system can be assessed by linearizing the systems about steady turning trajectories and performing eigen analysis. A review of the dominant eigenvectors

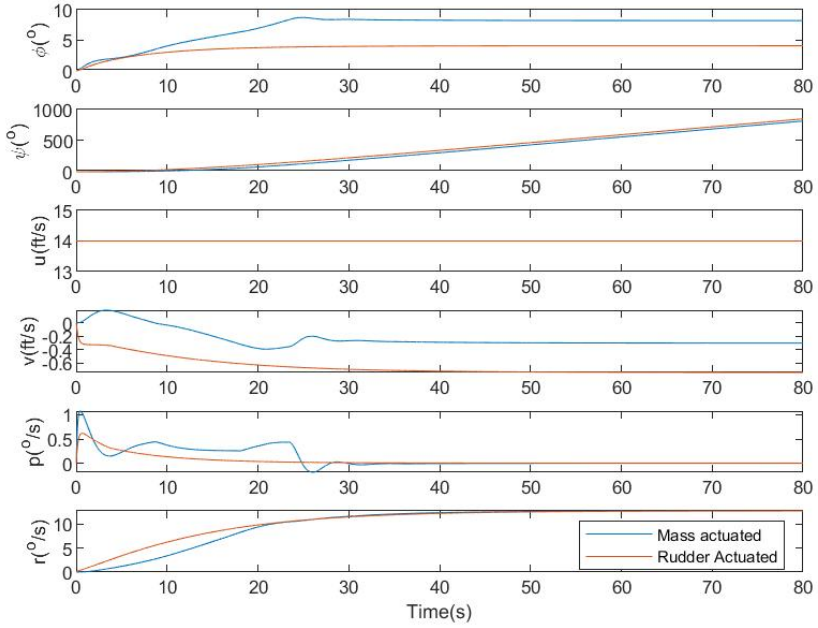

Figure 5.1: Deadrise 10°, Mass vs Rudder Actuated Turns: Mass of 10% of vessel at 0.3 ft starboard of centerline without a rudder in blue, mass amidship with rudder angle of -3.035° in red. With 10° deadrise, both have vcg of 0.25 ft, lcg of 1.2 ft from transom, and at fixed forward velocity with a Froude number of 3

and eigenvalues reveal dominant maneuvering characteristics.

A zero eigenvector is associated with free body motion about yaw in both models. This is intuitive since our equations of motion offer no spring force about the yaw degree of freedom where it the vessel is free to rotate. Next, both systems exhibit a similar highly damped non-oscillatory mode about the roll degree of freedom. Finally, we have a lightly damped oscillatory mode of combined roll, yaw, and sway degrees of freedom. These motions are categorized by Blount & Codega [5] likely as corkscrew or chine walking. The associated eigenvalues suggest a loss in stability associated with the lack of rudder. These modes are reasonable match our intuitive understand of maneuver motion.

Power required to maintain constant velocity during the turn using can be modeled as

	Eigenvalues						
	0	-7.5	-3.5		0	-7.6	-.42+1.1
	Eigenvectors						
p	-	0.13	-0.25		-	-0.13	.2+.6i
r	1	-	0.03		1	-	-.06+.04i
$\dot{v}$	-	-	0.38		-	-	.2+.001i
$\dot{p}$	-	-0.99	-0.88		-	0.99	-.74
$\dot{r}$	-	-	-0.09		-	-	-.1-.12i
	Rudder				Mass		

Table 5.2: Dominant eigenvectors and associated eigenvalues about linearized nodes of a model vessel of 10° deadrise simulated with rudder or mass maneuver methods

a product of the velocity with drag. Total drag is plotted, as well as rudder component for the rudder actuated system.

The mass actuated system initially poses less drag due to the lack of a rudder but increases as it settles into a steady turn. It is likely due to the increased asymmetry of the vessel's orientation to oncoming fluid as suggested by the larger heel angle in comparison with the rudder actuated turning model.

Finally for the 10° deadrise case, we considered a combined case using both a rudder and a mass varied on both port and starboard sides, evaluating power required to overcome drag at fixed velocity. The asymmetrical mass distribution affects heel and yaw rates due to positive N_ϕ as expected, but overall drag showed little difference from turning with just the rudder and a centered mass. Drag showed a linear dependency on yaw rate regardless of mass position and heel angle. Asymmetrical mass distribution did not yield appreciable drag savings.

In summary of 10° deadrise models where N_ϕ is positive, simulations show that using heel induced yaw moment enable maneuver without a rudder. This is achieved by placing

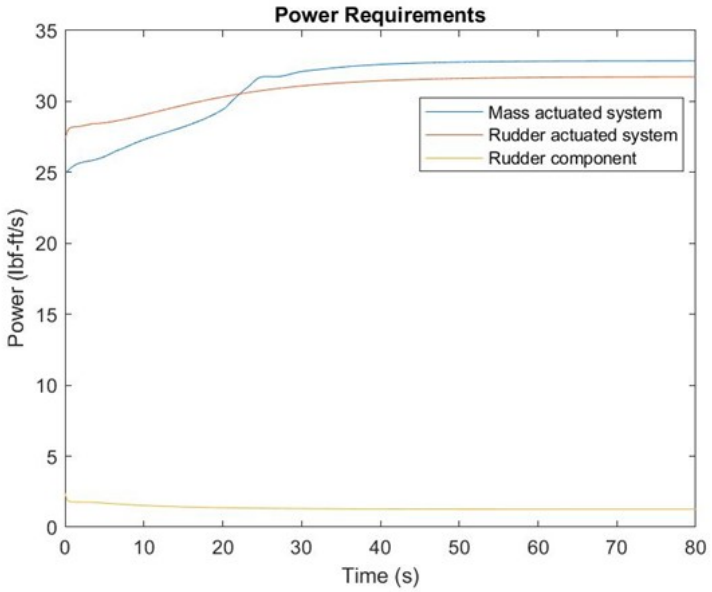

Figure 5.2: Drag Comparison: Power requirements to maintain constant velocity. Note that at straight trajectory, a mass actuated system exhibits less drag due to the lack of a rudder. The trend is reversed during steady turning

asymmetrical mass distribution to inboard since induced yaw moment is in the direction of heel. Though possible, rudder actuated turning has a quicker response, is more stable, and has lower overall power requirements in steady state turn. In combined rudder and asymmetrical mass use, steady heel and yaw rates showed cumulative effects of the different methods, but no savings in drag.

5.2 20° Deadrise

Next, consider a 20° deadrise model. Tests show that unlike the previous case of flatter bottom vessels, N_ϕ is negative. Because induced yaw moment is in the opposite direction of heel, let us consider placing asymmetrical mass distribution outboard to port with rudder actuation to starboard. In essence, mass effects would oppose rudder heel. Like the previous example, we compare the simulated trajectory to a rudder only model with advance, drag, and stability. Inputs were set to yield the same steady state yaw rates.

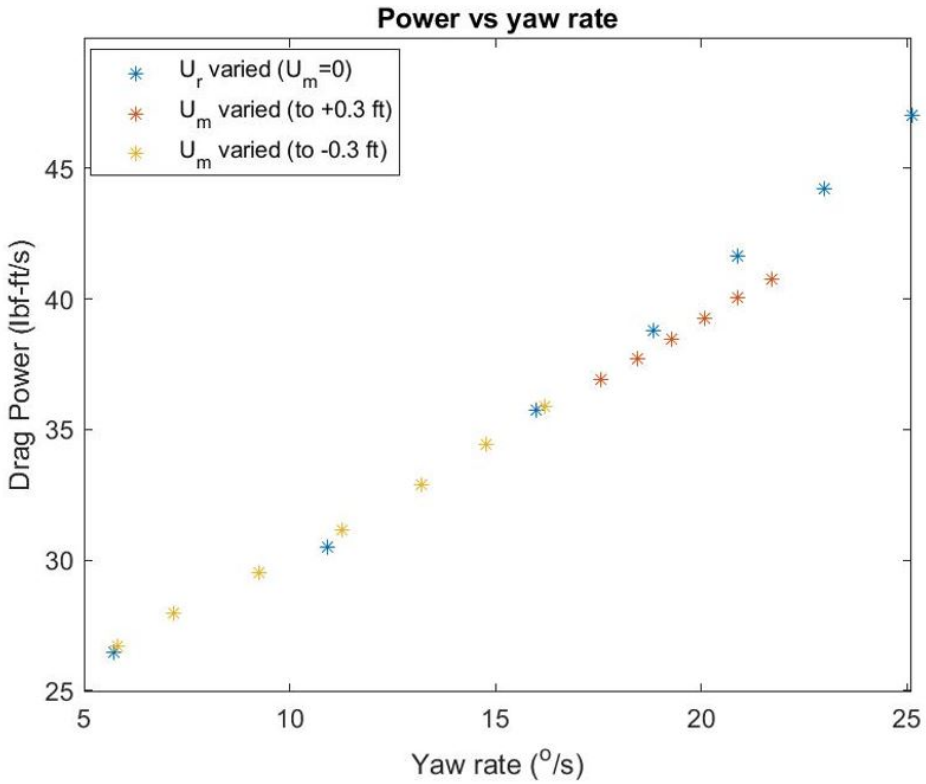

Figure 5.3: Drag Comparison: Comparison of drag for various rudder and mass positions for deadrise 10° vessel. Mass is placed centerline (blue), and in various positions to starboard (red) and port (yellow). Modeled drag force has a relatively linear dependency to yaw rate. In other words, for turning maneuver of flatter hull vessels, lateral asymmetrical mass distribution has little effect on drag

Model	Um (ft)	Ur (°)	r (°/s)
Rudder	0	-5.245	12.26
Mass & Rudder	-0.3	-3	12.26

Table 5.3: Control inputs resulting in the same steady turning rate of a model vessel of 20° deadrise

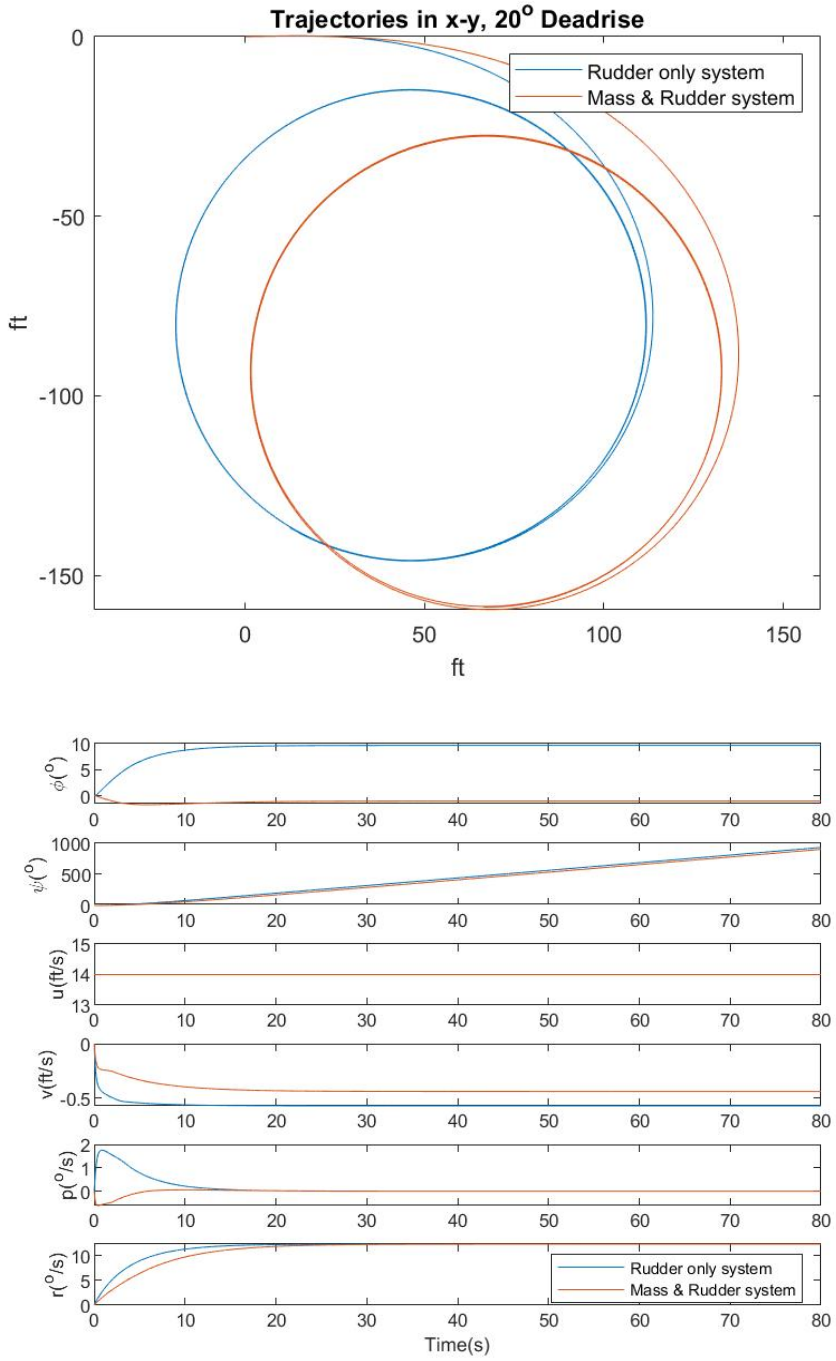

Figure 5.4: Deadrise 20°, Rudder Only vs Combined Mass & Rudder Actuated Turns. For combined system, mass of 10% of vessel at 0.3 ft port of centerline with rudder at -3° in red, with rudder only system with mass amidship with rudder angle of -5.245° in blue. Both have vcg of 0.25 ft, lcg of 1.2 ft from transom, and at fixed forward velocity with constant velocity

Comparing transient responses, the rudder actuated model exhibits a 17% shorter advance. Regarding heel, the control mass effectively opposes the roll moment induced by the rudder and minimizes heel.

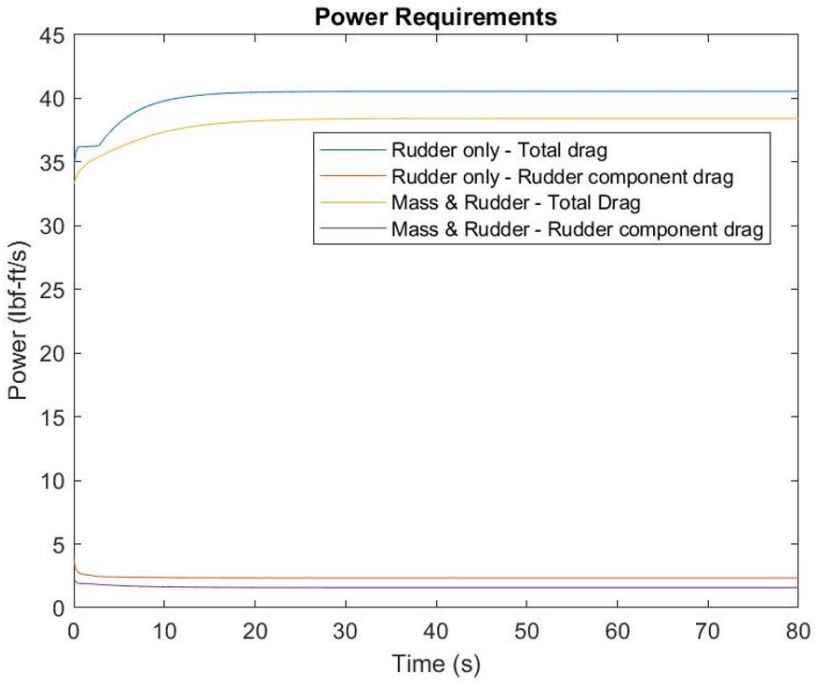

Figure 5.5: Drag Comparison: Power requirements to maintain constant velocity. Note that the combined mass & rudder actuated system exhibits less drag in all parts of the trajectory.

Total drag using combined mass & rudder method is less than rudder only in all parts of the trajectory and achieves 5% drag savings in steady turn.

For a vessel with a 20° deadrise using rudder only for maneuver, modal decomposition revealed similar modes to the 10° model consisting of a free yawing mode and a heavily damped roll mode. However, with a combined mass & rudder system, eigenvalues show increased stability with mass opposing heel. Eigenvectors lack of an oscillatory mode indicate the higher stability with higher deadrise.

	Eigenvalues					
	0	-6.1	-1.65	0	-6	-5.6
	Eigenvectors					
p	-	.17	-.51	-	.16	-.18
r	1	-	-.06	1	-	-
$\dot{v}$	-	-	-.12	-	-	-
$\dot{p}$	-	-0.99	.84	-	-.99	-.98
$\dot{r}$	-	-	.1	-	-	-
	Rudder			Mass & Rudder		

Table 5.4: Dominant eigenvectors & eigenvalues about linearized nodes of a model vessel of 20° deadrise simulated with rudder and combined mass & rudder maneuver methods. This indicates a higher level of stability using an asymmetrical mass in a position that counters rudder-induced heel

5.3 Optimization Potential for Drag

Countering or reducing the heel essentially allows a higher turn rate with reduced drag. This effect is found to in all situations where N_ϕ is negative, but most pronounced at high trim conditions. Simulating steady turns at constant velocity with a high trim angle at 5.9° and mass centered, increasing rudder angle increases yaw rates, heel, and drag as expected. By affixing the rudder at an arbitrary point and moving the mass to counter act heel, the yaw rate is increased with a savings in drag in comparison with a centered mass trajectory. Optimization using this method shows the potential to achieve a drag savings of 10%.

Time domain simulations were conducted to evaluate the potential for asymmetrical mass distribution to affect maneuver. At 10° deadrise with positive N_ϕ conditions, simulations show maneuver is possible without a rudder by capitalizing on the heel induced yaw moment from asymmetrical mass distribution only. In comparison to using a rudder, the mass method has lower drag in straight trajectory, greater drag during steady turning, and the cost of

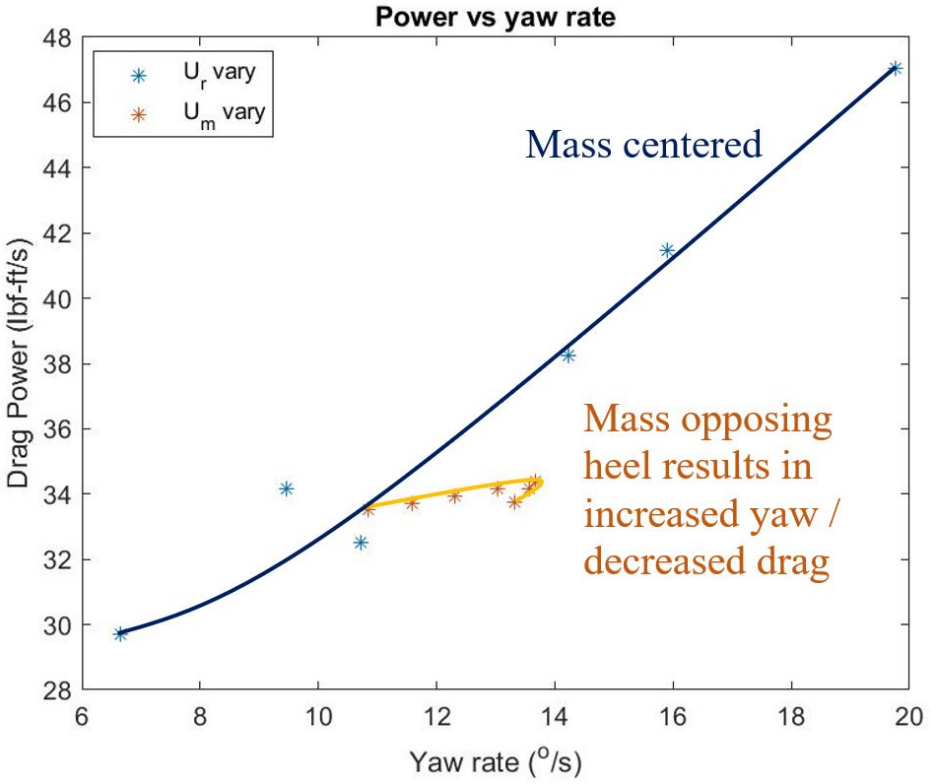

Figure 5.6: Optimizing Attitude: Increasing rudder angle results in increasing yaw rate and steady heel angle fit (blue). With rudder fixed, varying mass location to counter rudder induced heel effectively also increases yaw rate (orange). Simulations show convex behavior and an ideal heel angle of 5° for maximum yaw for given conditions of 20° and 5.9° trim angle

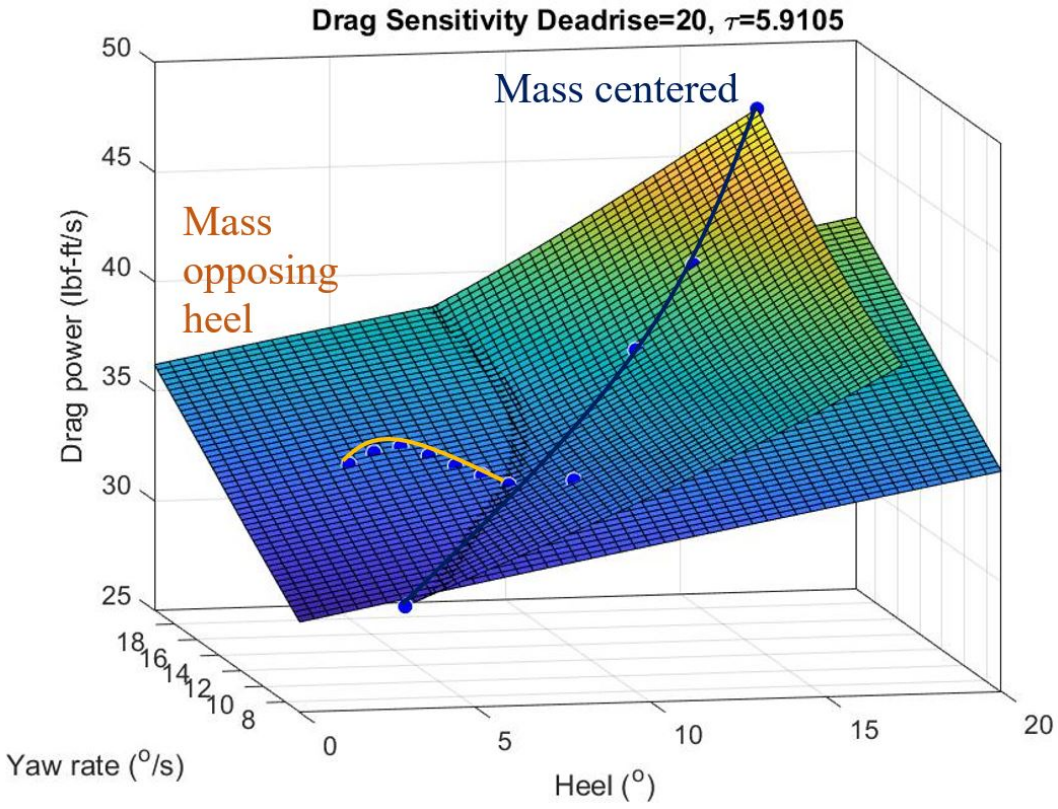

Figure 5.7: Optimizing Manifolds: Plots of drag, yaw rate, and heel establish 3D manifolds. The manifold of steeper slope represents the mass centered trajectory, while the flatter slope represents a mass opposing heel. Drag reduction is due to asymmetrical mass countering rudder induced heel (orange). In comparison with mass centered turning (blue), the model at optimal heel angle achieves the same yaw rate with a drag power savings of 10%

energy necessary to attain a steady state turn is roughly equal. The advance of the mass model is 30% greater than of the rudder model indicating less maneuvering responsiveness. Analysis of the linearized systems shows the presence of lightly damped oscillatory modes in both rudder and mass actuated systems. Though mass distribution methods can turn a vessel of 10° deadrise without a rudder, the response is sluggish and without significant energy or stability advantages in comparison with rudder methods. Practically, this method may be useful when the rudder is disabled due to damage, in draft prohibitive situations, or if the tasking requires mostly straight trajectories.

At 20° deadrise with corresponding negative N_ϕ behavior, we found convincing advantages in a configuration using a combined mass and rudder system with the mass placed outboard of the turn. Simulations were conducted in comparison with rudder only. The mass effectively countered the rolling moment induced by the rudder and reduced heel angles. This resulted in drag savings of up to 10% and improved stability. In addition, it did not suffer loss of responsiveness to the same level as the 10° deadrise mass model. Practically, this method may be useful for USV long duration applications with limited energy supply and in survey or directed energy tasks where performance is dependent on maintaining the vessel's upright attitude and stability.

These results indicate that the asymmetrical mass distribution effects on vessel attitude has the potential to minimize drag, maximize stability, or to attain convex optimization to other desirable metrics. The position maximum yaw rate to drag ratio presented in the 20° deadrise vessel scenario will be used in the following section as a configuration basis to develop optimal control.

5.4 End Swap Spinout

Shown in the asymmetrical mass trajectory scenarios is the presence of a Roll-Sway-Yaw oscillatory mode. Such oscillations have the potential to cause a non-oscillatory such as an end swap spinout. A high roll or yaw transient may introduce ventilation to the propeller and cause a loss of thrust, drop in trim angle due to the rapid deceleration, and an unexpectedly

high yaw moment that spins the vessel out of control. Morabito explored "end swapping" effects, so named due to the stern swapping ends with the bow [45]. This has led to disastrous consequences and motivated investigation.

Due to the extreme nature of the forces involved, this is a challenging trajectory to model with traditional methods of potential flow-based models or CFD. The complexity generally makes CFD cost prohibitive, and it cannot be readily simulated with 2D+t methods since conditions involved would exceed the range for which these models are applicable. The extreme deceleration in x axis, negative trim angle, and subsequent high yaw moment would pose flow separation, lateral flow under the keel, and conditions outside of the inviscid assumptions inherent in a potential flow based 2D+t model [16]. Not achievable by other low-cost means, an interpolative based model proves to be the most suitable to provide a quick and general understanding of a vessel's maneuvering behavior, especially since experimental data is available for negative trim angle trajectories. The experiments of [8] include static drift tests with trim at -2°, where hydrodynamic forces are indicative of those felt during an end swap trajectory. Using this data, the interpolated model at -2° can be compared with 3° and 6° trim conditions and shows that a bow down condition is associated with drastic increases in N_v, perturbing yaw moment with crossflow.

Using this data, we can estimate an end swap trajectory with a time domain simulation of our interpolation-based model. Our approach is to first establish a steady turning maneuver like the previous example with a constant thrust and turning input. Then, at time t=10s, a condition of thrust loss and negative trim angle is imposed. Forward velocity previously held as a fixed steady state constant is allowed to decelerate according to the Morrison model of thrust and drag. The simulated vessel spins around and comes to rest.

The simulated trajectory matches our intuition and observations of end swap type maneuvering instabilities. To prevent the roll and sway condition that may lead to the ventilation of the propeller [45], we look toward active feedback control to maintain roll stability. As we have shown in the 20° deadrise asymmetrical mass trajectory analysis, mass distribution that counters rudder induced heel may reduce drag during a steady turn. An additional benefit

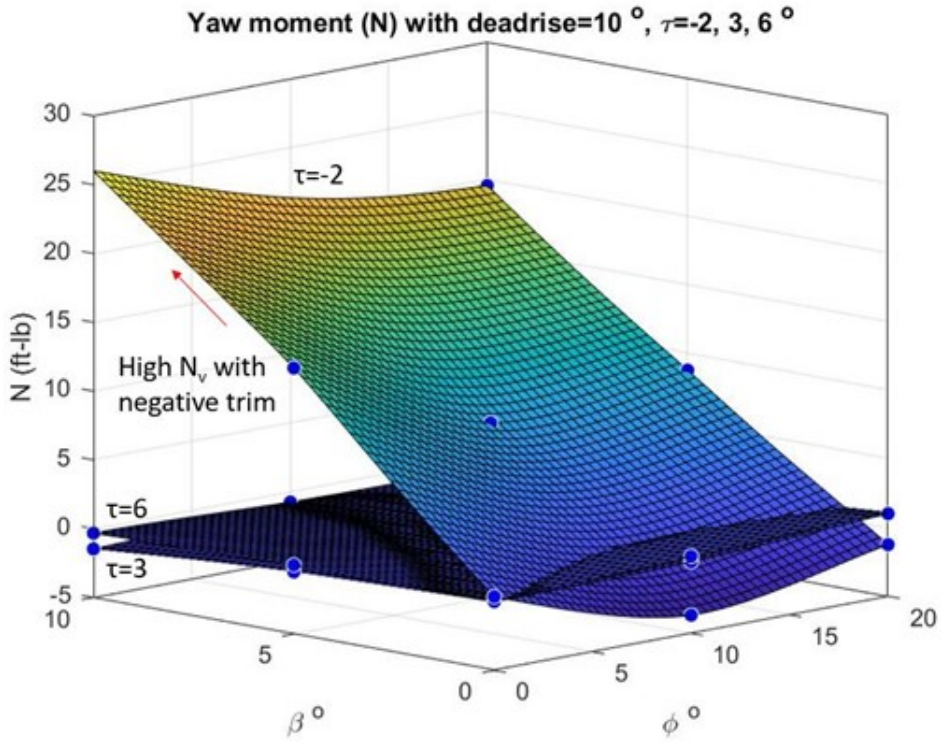

Figure 5.8: Behavior with Negative Trim: Yaw model shown at trim angles of 6°, 3°, and -2°. At negative trim angle as would be experienced in a rapid deceleration from planing velocities, we observe a higher order magnitude N_v perturbing yaw moment and results in extremely high yaw rates

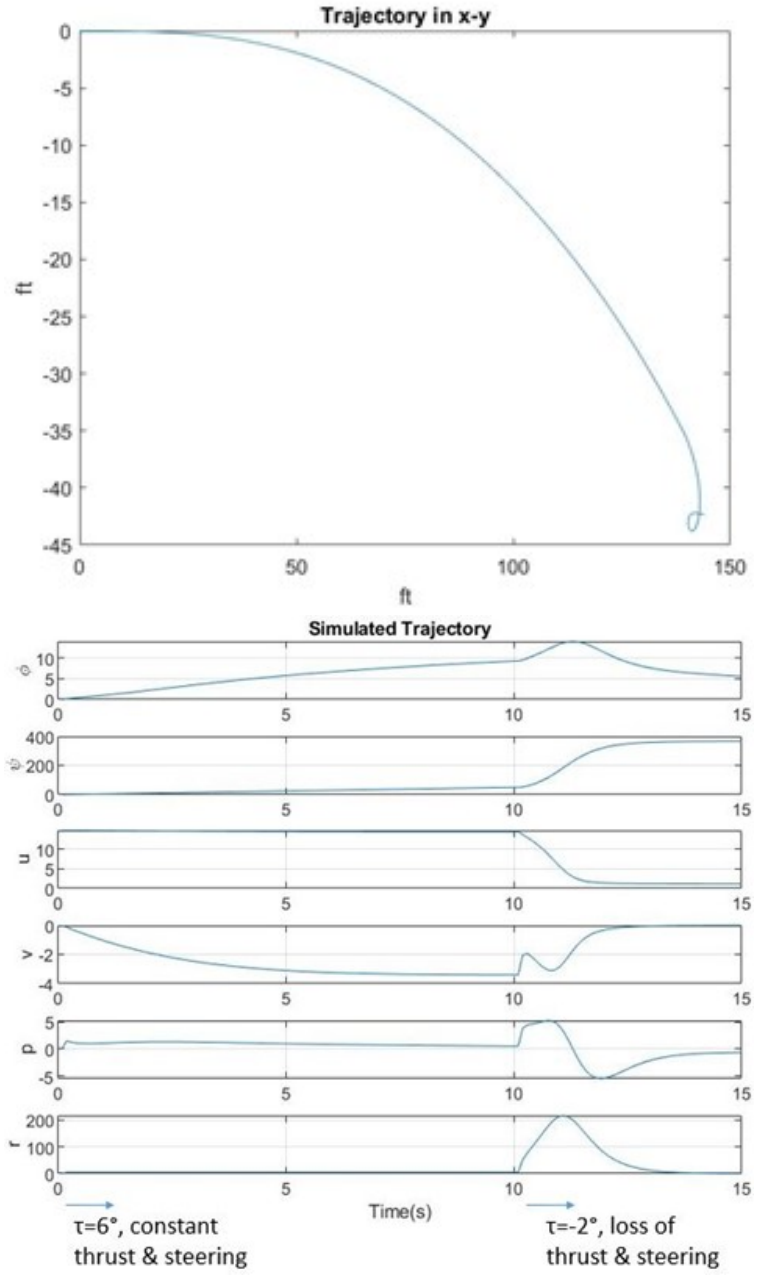

Figure 5.9: End Swap Trajectory: Time domain simulation of vessel in an end swap trajectory. Vessel develops a steady state starboard turn at 6° trim with constant thrust and turning input. At 10s, we simulate a loss of thrust and steering and a drop in bow to negative 2° trim. Dynamics associated with a negative bow condition result in extremely high yaw moment as evident by a rapid increase in yaw rate and an end swap spin as the vessel comes to rest

to reducing heel is an increase in stability margin from propeller cavitation and end swap instability. Extending out this concept, we next apply optimal feedback control to reduce roll as a means of instability avoidance.

5.5 Conclusion

A low-cost empirical and interpolation based prismatic planing vessel maneuver model with rudder was utilized to perform time domain simulations. We evaluated the potential for asymmetrical mass distribution to affect maneuver. At 10° deadrise with positive N_ϕ conditions, simulations show maneuver is possible without a rudder by capitalizing on the heel induced yaw moment from asymmetrical mass distribution only. In comparison to using a rudder, the mass method has lower drag in straight trajectory, greater drag during steady turning, and the cost of energy necessary to attain a steady state turn is roughly equal. The advance of the mass model is 30% greater than of the rudder model indicating less maneuvering responsiveness. Analysis of the linearized systems shows the presence of lightly damped oscillatory modes in both rudder and mass actuated systems. Though mass distribution methods can turn a vessel of 10° deadrise without a rudder, the response is sluggish and without significant energy or stability advantages in comparison with rudder methods. Practically, this method may be useful when the rudder is disabled due to damage, in draft prohibitive situations, or if the tasking requires mostly straight trajectories.

At 20° deadrise with corresponding negative N_ϕ behavior, we found convincing advantages in a configuration using a combined mass and rudder system with the mass placed outboard of the turn. Simulations were conducted in comparison with rudder only. The mass effectively countered the rolling moment induced by the rudder and reduced heel angles. This resulted in drag savings of up to 10% and improved stability. In addition, it did not suffer loss of responsiveness to the same level as the 10° deadrise mass model. Practically, this method may be useful for USV long duration applications with limited energy supply and in survey or directed energy tasks where performance is dependent on maintaining the vessel's upright attitude and stability.

Chapter 6

OPTIMAL ROLL STABILITY USING INERTIAL MASS

Compared to vertical plane heave-pitch oscillations called porpoising, horizontal plane oscillations are relatively less studied. Designers and vessel operators rely on empirically based guidelines with which to avoid undesirable conditions. Blount [5] observed that roll oscillations called "chine walking" occur without apparent excitation and offered guidelines to avoid instabilities based on full scale trials. Lewandowski [39] described these instabilities as a Roll–Yaw-Sway oscillatory mode and presented maximum KG for transverse dynamic stability. Based on experiments, Katayama [34] characterized the modal motion as Roll–pitch–heave rather than Roll-yaw-sway and proposed that they are caused by parametric resonance with vertical plane oscillations. Tascon [60] assumes this theory and a one-way coupling between heave-pitch and roll, and performs instability analysis using 2D+t based modeling. Vertical to horizontal plane force coupling effects on roll oscillations was further studied by Tavakoli [62] who proposes that heave freedom increases roll damping, also using 2D+t based modeling. The precise characterization of horizontal plane oscillations is complicated by the lack of high fidelity test data. Nevertheless, our model is able to add perspective of these oscillations, which we use to develop optimal feedback control.

Consider a solid mass Active Mass Actuator (AMA) with the ability to move linearly across a vessel's lateral axis for roll disturbance rejection. We seek to develop optimal control via a Linear Quadratic Regulator (LQR) and compare performance against a Rudder Roll Stabilizer (RRS). The three actuator configurations considered are:

- AMA actuation in a 5DOF model with fixed RRS position
- RRS actuation in a 4DOF model with fixed AMA position

- Combined AMA and RRS in a 5DOF model with actuation of both AMA and RRS

First, the system is linearized about a pre-determined optimal equilibrium turning trajectory with fixed control inputs discussed in section 5.3. Let $\bar{\nu}$ represent an equilibrium state, $\bar{u}$ the fixed input positions associated with that equilibrium, and f our nonlinear system dynamics. Linear system matrices A_{lin} and B_{lin} are obtained by performing Jacobians numerically about that equilibrium.

$$A_{lin} = \frac{\partial f}{\partial \nu}|_{\bar{\nu},\bar{u}},\ B_{lin} = \frac{\partial f}{\partial u}|_{\bar{\nu},\bar{u}} \tag{6.1}$$

This would set up our desired continuous time linear time-invariant system.

$$\dot{\nu} = A_{lin}\nu + B_{lin}u \tag{6.2}$$

6.1 Feedback via a Linear Quadratic Regulator

The objective is to stabilize the vessel by regulation of state variables with a minimum of control action on an infinite time horizon:

$$J = \int_0^\infty x(\tau)^T Q x(\tau) + u(\tau)^T R u(\tau)\ d\tau \tag{6.3}$$

The strategy we employ to assign the cost of state weight matrix Q is inspired by the modal decomposition of the open loop response [28]. The normalized values of the eigenvector most closely corresponding to a roll-sway-yaw "chine-walking" mode are directly assigned as the diagonal values of Q. Controller cost matrix R is chosen so that the range of the response does not exceed actuator saturation limits.

Solving the Riccati equation results in optimal state feedback law and provides ability to close the loop:

$$u(t) = K(\bar{\nu} - \nu) \tag{6.4}$$

$$\dot{\nu} = (A_{lin} - B_{lin}K)\nu \tag{6.5}$$

Linear closed loop dynamics are provided by [eq: 6.5]. Optimal gain matrix K can be modified to represent less-than-full state feedback. States of ϕ, p, r, and AMA position are key to stability and performance. Because roll and yaw are coupled, minimizing errors on ϕ directly affect ability to maintain yaw rate. Observing roll rate p provides ability to maintain stability it the presence of roll disturbances. Finally, model decomposition indicates a dominant value in AMA position in stability. Only gains associated with representative observable states of these mentioned states are retained and the rest are zeroed out.

Linear analysis on closed loop linear model [eq. 6.5] provides indication on stability and controller performance using these methods. Nonlinear performance can also be assessed by using the control law [eq. 6.4] in the nonlinear model [eq. 2.33] and numerically simulating in time domain simulation.

6.2 Closed Loop Linear Analysis

After optimal rudder and/or AMA positions are determining, equilibrium can be modeled through numerical simulation of the nonlinear equations of motion until the transient accelerations die out and we attain a steady heel angle and yaw rate. For the sake of demonstration, let us consider a 20° deadrise vessel identical to the experimental hull used in [8] with length of 50 inches and beam of 9 inches. Let the rudder angle be fixed at -4° (to starboard), and AMA lateral position at -0.15 ft (1.8 in starboard of centerline), 0.1 ft above the center of gravity, with vessel lcg 1.5 ft from transom. This corresponds to a mass position that op-

poses rudder induced heel moment and establishes a pre-determined optimal orientation to minimize drag during a starboard turn. Nonlinear equations of motion in 4DOF [eq. 2.25] are integrated using MATLAB ODE15s function from straight trajectory initial conditions until vessels settles into a steady turn to starboard. Equilibrium is determined to be at 6.04° heel, sway velocity of 0.54 ft to port, and a trim angle of 3.52°.

Nonlinear dynamics are linearized about equilibrium state. If AMA active feedback is considered, a 5DOF system is used; if not, the system remains in 4DOF with the AMA position fixed. Optimal control laws and closed loop linear systems are established for the three actuator configurations mentioned. Open and closed loop system zeros, poles, and associated eigenvalues determined through modal decomposition are analyzed to provide qualitative insight into response characteristics of the systems as shown in [Fig. 6.1].

The existence of a zero in the right hand plane of both the open loop system provides indication that 1) the presence of familiar dynamics inherent to fin-type control mechanism and 2) a non-minimum phase that would pose potential fundamental limitations associated with the RRS only system, especially in high frequency responses. The closed loop RRS system not only has the same right hand plane zero, but also contains a problematic near coincident oscillatory pole and zero. Combined with time delays of physical RRS actuators and bandwidth limitations, these indicators point to reduced limits to achievable performance [15].

Bode plots of these systems shown in [Fig. 6.2] provide measure of roll disturbance rejection across the frequency domain. The output is set to heel angle ϕ and input of disturbing roll moment. Performance using AMA as a mechanism for roll disturbance rejection results in approximately 10dB improvement over RRS.

6.3 Closed Loop Nonlinear Simulation

To assess controller performance on non-linear systems, time domain trajectories are simulated. A perturbation about the equilibrium state in the direction of a chine-walking oscillation is established in the initial conditions.

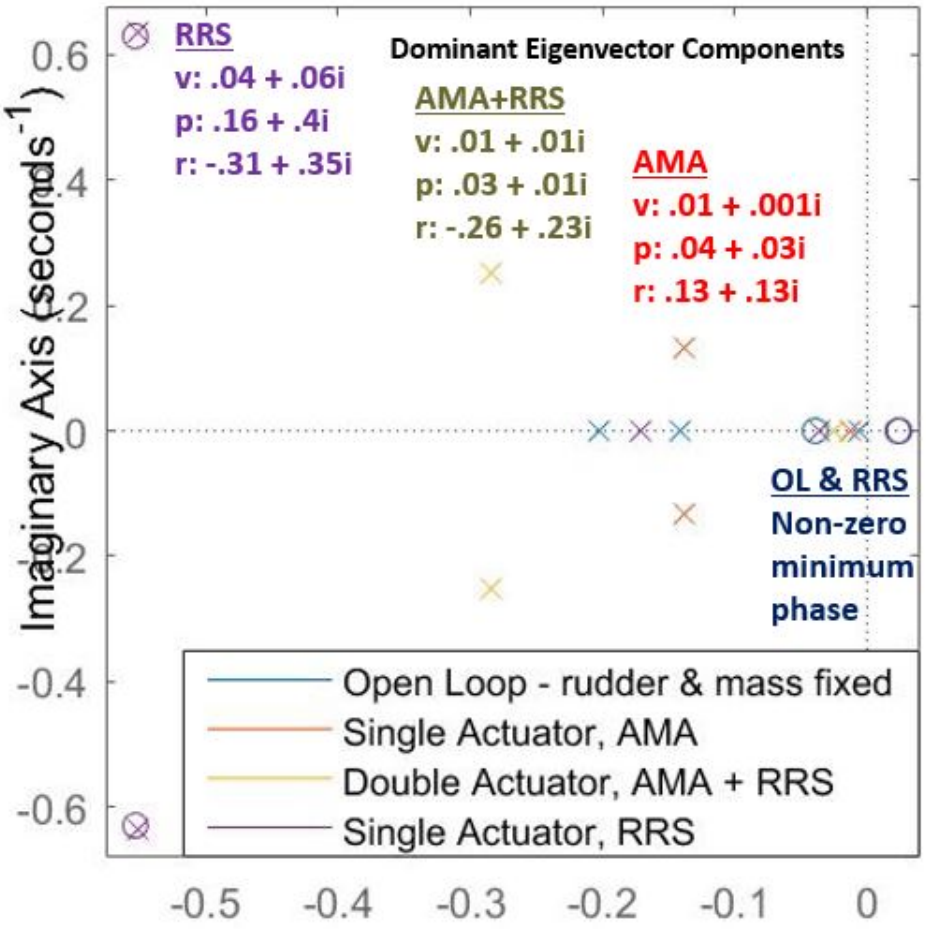

Figure 6.1: Pole Zero Analysis: Poles and zeros closest to the origin of open loop and closed loop systems. Note the relevant components of eigenvectors associated oscillatory zeros indicate a chinewalking mode in roll-sway-yaw, and the open loop and RRS closed loop systems have a right hand plane zero.

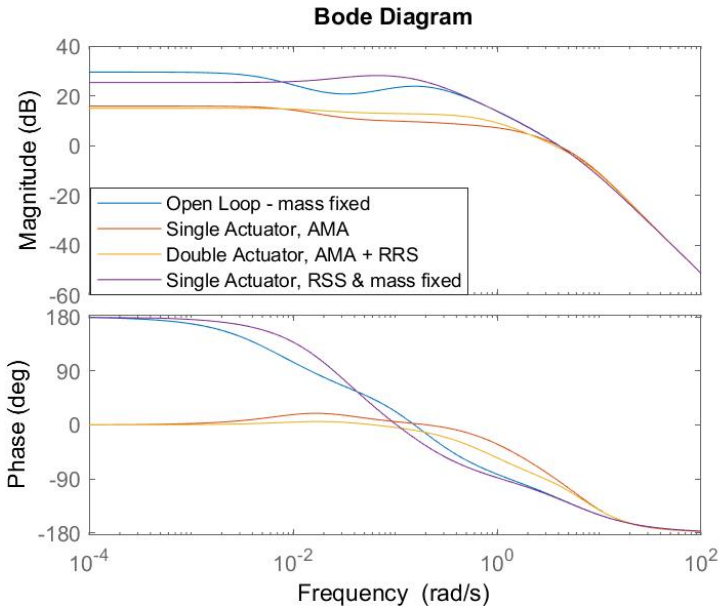

Figure 6.2: Bode Analysis: Bode frequency plot showing roll disturbance responses. Inertial mass methods have approximately 10dB better performance in roll disturbance rejection compared with rudder methods.

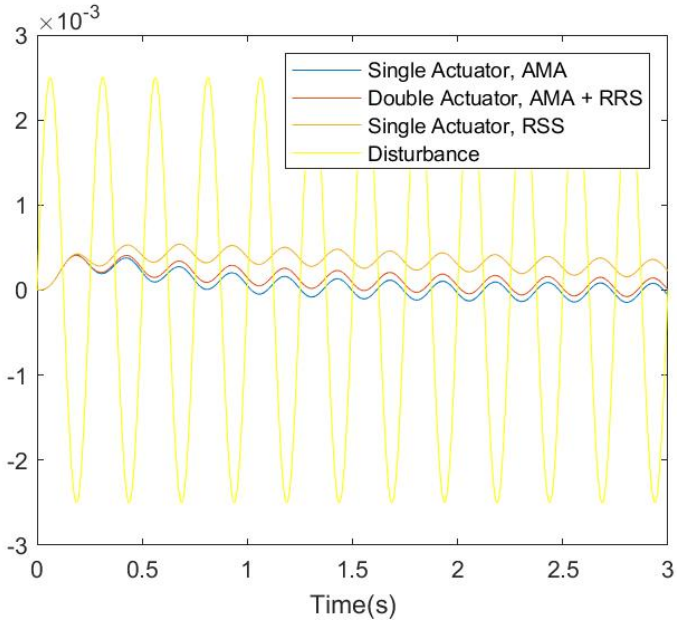

Figure 6.3: Linearized Response: Time domain response of linearized systems to sinusoidal roll disturbance

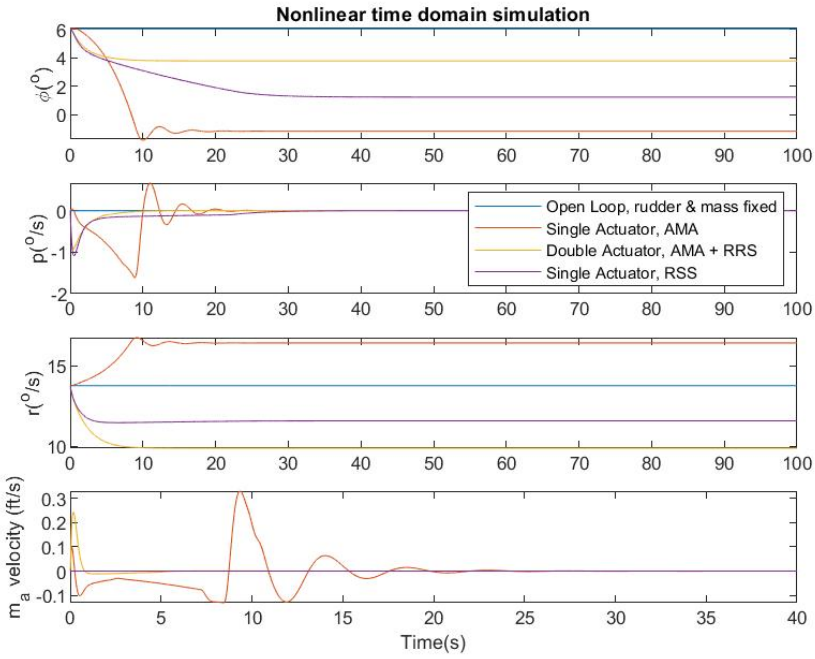

Figure 6.4: Nonlinear Response: time domain trajectories

As illustrated in [Fig. 6.4], all seakeeping actuation methods presented demonstrate the ability stabilize the transient caused by the initial perturbation. Maximum velocities of the AMA are less than 0.4 ft/s as a result to the weights assigned to actuator cost.

The actuator mechanisms are able to deliver adequate roll damping to maintain stability given the initial perturbation. However, due to roll yaw coupling and rigid body mode about yaw, the response also establishes a new equilibrium. This is seen in the steady roll angle and yaw rate errors that the responses develop [Fig. 6.5]. This method of roll control may be best suited to work in conjunction with a maneuver controller focused on yaw state reference tracking. Since re-establishing reference yaw rate is a separate objective, it may be best be addressed back in the maneuver controller using such classic strategies as PID or Nomoto algorithm [23]. The concept of composite control involving slow control for maneuver objectives and a fast control for seakeeping was studied with RRS [14] [22]. This

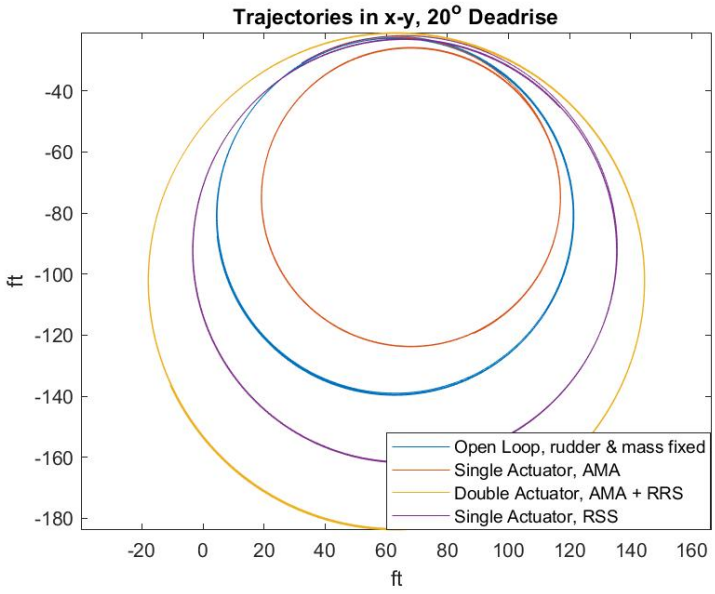

Figure 6.5: Nonlinear XY trajectory: plots show that the roll stability measures presented are capable of re-establishing steady turns given an initial perturbation, though new equilibrium states result due to the coupling between roll and yaw

would serve useful in our application as well as illustrated in our concept controller on Figure 6.6. Thus, the methods presented provide improve roll control and seakeeping capability for planing vessels while fitting in the context of existing theory and other solutions that can better address yaw reference tracking error.

6.4 Limitations & Design considerations

The wide spectrum of potential environmental disturbances faced by displacement vessels is even further widened in the planing regime due to the velocity of the vessel. Factoring in the incipient velocity of a high speed vessel, wave frequency, and actuation time delay, the actuator will require greater speed and precision than those applied to RRS systems on displacement vessels. Frequency of wave disturbances experienced by the vessel as a function of forward velocity, wave spectrum, and angle of encounter is described by [23]:

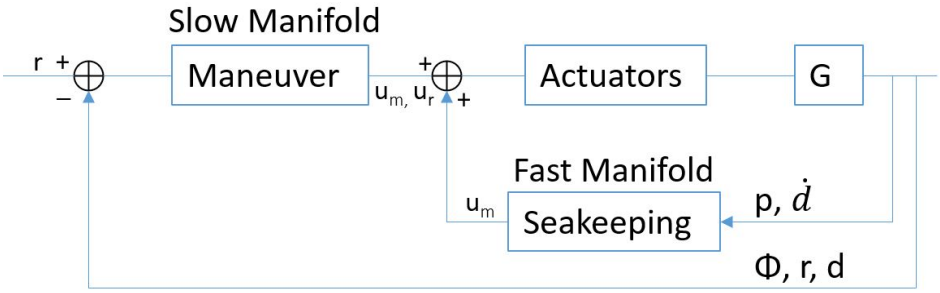

Figure 6.6: Concept Control Design: uses techniques presented and yaw reference tracking via a classic maneuver controller. u_r and u_m are control inputs to RRS and AMA respectfully. Segregation of time horizons differentiate the desired response since roll disturbance generally acts faster than maneuver signals. Seakeeping controller minimizes roll and AMA velocity while Maneuver controller determines mean actuator positions to minimize error in steady yaw rate and heel.

$$\omega_e = \omega_0 - \frac{\omega_0^2}{g} U cos(\beta) \tag{6.6}$$

Consider newly developed seas with a short period T=4 s waves disturbance, equating to a frequency of 1.57 rad/s. Assuming the wave height are low enough that our model vessel stays at the water's surface, the frequency experienced by our representative planing vessel model will be the highest at 2.43 rad/s with the vessel moving against the direction of the waves. Given roll disturbances at that frequency, an AMA actuator would need to operate faster than for displacement vessel in the same environment. This motivates a robust approach that is able to factor disturbances, sensor noise, and model uncertainty to evaluate the bounds of applicability.

Inherent in interpolative based modeling, accuracy is dependent on the underlying test data. The methods demonstrated in this paper rely on a rigorously developed but fairly sparse data set. Additional testing that establishes high fidelity data would enable higher degrees of accuracy and enable characterization of model uncertainty. Free running tests on asymmetrically loaded planing vessels could both enhance our understanding of horizontal

plane instabilities and positively demonstrate the use of roll-yaw coupling for maneuvering objectives. Finally, because the methods shown were developed in 4DOF for model dynamics, effects of heave and pitch and not considered. Expanding the model to 6DOF would enable a higher level dynamic representation.

6.5 Conclusion

The proliferation of small high speed USVs motivates the study of new inertial based control methods. We consider a solid mass of 10% vessel weight with the ability to move laterally within the vessel hull. This may be representative of a lithium battery powering a small prismatic planing hull USV. A 5DOF model is established to characterize the vessel - control mass motions in maneuver and roll in full planing dynamic regime. Hydrodynamic forces are estimated using a low computational cost method based on test data interpolation that enables the development of controls.

A Linear Quadratic Regulator (LQR) is applied and the closed loop Active Mass Actuator (AMA) system is evaluated against a Rudder Roll Stabilization (RRS) system. While both system responses contained a damped oscillatory mode in Roll-Sway-Yaw characterized as chine-walking, the RRS responses also yield a right hand plane zero and a coincident pole zero. This suggests a fundamental limitation to performance of the RRS system on a planing vessel and an advantage of the AMA system due to a lack of those limitations. In addition, linear analysis show a 10 dB better performance in roll disturbance rejection on the AMA system. Nonlinear time-domain simulations indicate that closed loop response to perturbations may result in steady yaw reference tracking error. This is understandable given the roll-yaw coupling of planing vessels and rigid body mode about yaw, and suggests that this method of roll control is best paired with a maneuver controller to address tracking error.

This numerical demonstration suggests that active distribution of inertial mass methods can exploit the roll-yaw coupling of planing vessels to affect both roll control and turning. Thus, inertial mass methods can be utilized to meet both seakeeping and maneuver objectives and eliminate the need for traditional external fin type control mechanisms such as a rudder.

This can be advantageous in drag reduction, allowing shallow water access, and in other situations that disfavor rudders.

To further validate this concept, we recommend a few lines of effort. First, free running experiments with asymmetrical mass distribution would provide high fidelity data to enhance our interpolative based model and provide quantitative measure of uncertainty. Second, factor uncertainty, noise, actuator delay, and noise in a robust approach toward control design. Finally, enhance the model to consider all degrees of freedom and consider the effects of pitch and heave.

Chapter 7

CONTRIBUTION AND RECOMMENDATIONS

In this paper, we gain new insights into motion control for prismatic planing hulls between 10° and 20° deadrise. The essential dynamic explored is the coupling between roll, sway, trim, and yaw. By establishing a low cost model that captures those dynamics, we enable new ideas that exploit that dynamic coupling for maneuvering and seakeeping objectives.

Like an aircraft, planing hulls are supported by lift. We showed through numerical simulation that a low deadrise vessel can turn without the use of a rudder by using the roll moment from asymmetrical mass loading to induce yaw. For higher deadrise vessels, mass loading that opposes rudder induced heel result in overall reduction in drag. The position of the mass can be optimized to yield up to 10% drag savings and improve stability. We extend the concept of seakeeping to maintain planing vessel stability in a stable turn. Linear analysis reveals the potential for chine-walking oscillations to be in a roll-sway-yaw mode which challenge recent studies that describe them as a roll-heave-pitch. Optimal closed loop feedback applied to an inertial mass with free lateral movement showed improved performance characteristics compared with rudder roll stabilization methods.

This demonstrates a process of applying interpolated test data, empirical equations, and simplifying assumptions to drastically reduce computational requirements to achieve desired insight and control applicability. As higher fidelity experimental data becomes available, this process is scalable to incorporate the data for higher accuracy and capture additional dynamics. With a 10% of vessel mass used as an inertial control mass, it is notable that simulations show a drag savings up to 10% with 10 db better performance than rudder methods in roll rejection; the multiple of 10's indicate a potential for scaling effects. We have demonstrated focus on roll-yaw dynamic coupling and a level of optimization through

the geometric parameter of deadrise. However, scaling effects and sensitivity to inertial mass size, vertical placement, and other design parameters will be useful in exploring co-designed geometry and control features. Finally, because of the low cost, this method may have particular utility in such applications as Model Predictive Control.

7.1 Recommendations for Future Work

Future experimental studies could unlock potential along the following levels of effort:

- Free running tests: Use high fidelity sensors to capture full state measurements on a free running prismatic planing hull with an asymmetrical mass distribution. Results can be evaluated using system ID methods such as described. [10]. This could capture additional coupled dynamics in including heave and pitch in higher accuracy. Also, high fidelity data would enable quantification of model uncertainty.

- Improve control methods: This can be pursued along a few different approaches. Using Model Predictive Control [49] [50] [20] can be utilized in conjunction with onboard forecasting of the vessel's hydrodynamic forces [29] to determine optimal control laws. A robust approach would offer consideration of quantified model uncertainty, actuator tolerances in accuracy and time delay, sensor noise, and environmental disturbance in optimization. Tanguy [59] demonstrates a H_∞ application to roll control. This may develop understanding of this method's applicability to other similar shaped hull design for which we do not have experimental data.

- Expansion of model to include heave and pitch: Experiments by Bonci [6] indicate significant variations to the behavior of roll-yaw coupling with changes in position of the vessel in a wave. In the context of the results of this paper, it can be reasoned that pitch-heave coupling may be responsible. Thus, while our isolated treatment of roll-yaw has produced useful results, expanding the model to a vessel 6DOF would be required to consider the necessary dynamics in waves.

- Co-designed optimization of trajectory and controls: Perform sensitivity analysis on inertial mass size and vertical position to estabilish theory on scaling effects and performance of optimization. A few researchers have applied genetic algorithm in optimization of controls and vessel geometries. Castro-Feliciano [12] [13], has applied it in optimization of codesigned vessel geometry and LQR parameters, using the Powersea commercial modeling program. Masumi [42] applied it to both longitudinal and transverse stability using empirical models of Savitsky and Lewandowski. Such methods in application to our model would expand the utility to both maneuver and seakeeping optimization on the basis of drag and stability. Optimal trajectory states can be then input into a concept control design as shown on Figure 6.6 applying slow control on maneuver and fast control on seakeeping [14].

- Stability analysis: using free running test platform, mimic chine-walking oscillations with high fidelity sensors. Improved characterization of instabilities would enhance the control approach toward mitigating them.

- Investigate the sensitivity of added mass model to time varying parameters: Empirical methods exist [31] developed by Judge to account for time varying roll changing wetted surface properties. Using these methods would provide a time varying added mass formulation. Thus, a sensitivity analysis would yield indication on the importance of capturing time variance.

- Sway effects on wetted surface: While Judge [31] captured wetted surface effects of roll, this process can be extended to capture sway as well. That would offer a full suite of empirical tools that would enable higher accuracy in time varying added mass and damping models.

These are a few recommendations that would better accuracy, high dynamics, an improved understanding of the instabilities, and enable robust control.

BIBLIOGRAPHY

[1] Martin A Abkowitz. Measurement of hydrodynamic characteristics from ship maneuvering trials by system identification. Technical report, 1980.

[2] Roberto Algarín and Antonio Bula. A numeric study of the maneuverability of planing hulls with six degrees of freedom. *Ocean Engineering*, 221(July 2020):108514, 2021.

[3] AAM Ayob and O Yaakob. Roll mitigation of small fishing boat. *Journal of Transport System Engineering*, 2(2):46–50, 2015.

[4] Ahmad F Mohamad Ayob, Tapabrata Ray, and Warren F Smith. Beyond hydrodynamic design optimization of planing craft. *Journal of Ship Production*, 27(1):1–13, 2011.

[5] D Blount and L Codega. Dynamic Stability of Planing Boats. *Marine Technology and SNAME News*, 29(01):4–12, 1992.

[6] M. Bonci, P. De Jong, F. Van Walree, M. R. Renilson, and R. H.M. Huijsmans. The steering and course keeping qualities of high-speed craft and the inception of dynamic instabilities in the following sea. *Ocean Engineering*, 194(July):106636, 2019.

[7] Jeffrey Bowles. Turning characteristics and capabilities of high-speed monohulls. *3rd Chesapeake Power Boat Symposium, CPBS 2012*, (June):1–18, 2012.

[8] P Ward Brown and Walter E Klosinski. Directional stability tests of two prismatic planing hulls. Technical report, 1994.

[9] P. Ward Brown and Walter E. Klosinski. Experimental Determination of the Added Inertia and Damping of Planing Boats in Roll. 1995.

[10] Steven L. Brunton, Joshua L. Proctor, J. Nathan Kutz, and William Bialek. Discovering governing equations from data by sparse identification of nonlinear dynamical systems. *Proceedings of the National Academy of Sciences of the United States of America*, 113(15):3932–3937, 2016.

[11] Steven L. Brunton1, Joshua L. Proctor2, and J. Nathan Kutz3. Supporting Information for: Discovering governing equations from data: Sparse identification of nonlinear dynamical systems. *Nature Communications*, 8(1):1–38, 2017.

[12] Esteban L Castro-Feliciano, Jing Sun, and Armin W Troesch. First step toward the codesign of planing craft and active control systems. *Journal of Offshore Mechanics and Arctic Engineering*, 139(1), 2017.

[13] Esteban L Castro-Feliciano, Jing Sun, Armin W Troesch, Matthew Collette, et al. Codesign case study of a planing craft with active control systems. *Journal of Ship Research*, 63(03):182–197, 2019.

[14] Shyh Leh Chen, Steven W. Shaw, Hassan K. Khalil, and Armin W. Troesch. Robust stabilization of large amplitude ship rolling in beam seas. *Journal of Dynamic Systems, Measurement and Control, Transactions of the ASME*, 122(1):108–113, 2000.

[15] Swarup Das. Rudder Roll Stabilisation : An Perspective Rudder Roll Stabilisation : An Perspective. (June), 2014.

[16] Abbas Dashtimansh, Hossein Enshaei, and Sasan Tavakoli. Oblique-Asymmetric 2D1T Model to Compute Hydrodynamic Forces and Moments in Coupled Sway, Roll, and Yaw Motions of Planing Hulls. *Journal of Ship Research*, 49(4):233, 2019.

[17] Barry Deakin. Model tests to assess the manoeuvring of planing craft. In *The International HISWA Symposium on Yacht Design and Yacht Construction*, pages 21–32, 2005.

[18] Sukru Akif Erturk and Atilla Dogan. Dynamic simulation and control of mass-actuated airplane. *Journal of Guidance, Control, and Dynamics*, 40(8):1939–1953, 2017.

[19] Sukru Akif Erturk and Atilla Dogan. Relative controllability evaluation of mass-actuated airplane. *Journal of Guidance, Control, and Dynamics*, 42(2):384–393, 2019.

[20] H. N. Esfahani and R. Szlapczynski. Rudder roll damping and ship heading control using a model predictive control algorithm. *Developments in the Collision and Grounding of Ships and Offshore Structures - Proceedings of the 8th International Conference on Collision and Grounding of Ships and Offshore Structures, ICCGS 2019*, (October):377–383, 2020.

[21] Odd M Faltinsen. *Hydrodynamics of high-speed marine vehicles*. Cambridge university press, 2005.

[22] Thor I. Fossen. A survey on Nonlinear Ship Control: from Theory to Practice. *IFAC Proceedings Volumes*, 33(21):1–16, 2000.

[23] Thor I Fossen. *Handbook of marine craft hydrodynamics and motion control*. John Wiley & Sons, 2011.

[24] Karl Garme. Improved time domain simulation of planing hulls in waves by correction of the near-transom lift. *International Shipbuilding Progress*, 52(3):201–230, 2005.

[25] Parviz Ghadimi, Sasan Tavakoli, Abbas Dashtimanesh, and Pouria Taghikhani. Dynamic response of a wedge through asymmetric free fall in 2 degrees of freedom. *Proceedings of the Institution of Mechanical Engineers Part M: Journal of Engineering for the Maritime Environment*, 233(1):229–250, 2019.

[26] Benjamin Golding, Andrew Ross, and Thor I. Fossen. Identification of Nonlinear Viscous Damping for Marine Vessels. *IFAC Proceedings Volumes*, 39(1):332–337, 2006.

[27] S. Hajizadeh, M. S. Seif, and H. Mehdigholi. Determination of ship maneuvering hydrodynamic coefficients using system identification technique based on free-running model test. *Scientia Iranica*, 23(5):2154–2165, 2016.

[28] Amir Hossein Heidari, Sadegh Etedali, and Mohamad Reza Javaheri-Tafti. A hybrid LQR-PID control design for seismic control of buildings equipped with ATMD. *Frontiers of Structural and Civil Engineering*, 12(1):44–57, 2018.

[29] Limin Huang, Yang Han, Wenyang Duan, Yi Zheng, and Shan Ma. The gyroscopic effects of flying weels on board ship. *Ocean Engineering*, 164(February):212–227, 2018.

[30] Myung-Jun Jeon, Dong-Hyun Lee, and Hyeon-Kyu Yoon. Development of 6-DOF Equations of Motion for a Planning Boat Based on the Results of Sea Trial Tests. *Journal of Navigation and Port Research*, 40(5):231–239, 2016.

[31] Carolyn Q. Judge. Coupling of heave and roll for high-speed planing hulls. *Proceedings of the International Conference on Offshore Mechanics and Arctic Engineering - OMAE*, 8A:1–6, 2014.

[32] Carolyn Q. Judge. Empirical methods for predicting lift and heel moment for a heeled planing hull. *Journal of Ship Production and Design*, 30(2):1–9, 2014.

[33] Carolyn Q. Judge and John A. Judge. Measurement of hydrodynamic coefficients on a planing hull using forced roll oscillations. *Journal of Ship Research*, 57(2):112–124, 2013.

[34] Toru Katayama. Experimental Techniques to Assess Dynamic Instability of High-Speed Planing Craft - Non-zero Heel , Bow-Diving , Porpoising and Transverse Porpoising -. *Time*, (January 2002):1–9, 1988.

[35] Toru Katayama and Tomoki Taniguchi. Development of maneuvering simulation method for high speed craft using hydrodynamic forces obtained from model tests. *10th International Conference on Fast Sea Transportation FAST 2009*, (October):477–489, 2009.

[36] Dong Jin Kim and Sun Young Kim. Turning characteristics of waterjet propelled planing boat at semi-planing speeds. *Ocean Engineering*, 143:24–33, 2017.

[37] K.S. Kula. An Overview of Roll Stabilizers and Systems for Their Control. *TransNav, the International Journal on Marine Navigation and Safety of Sea Transportation*, 9(3):405–414, 2015.

[38] Edward Lewandowski. *The Dynamics of Marine Craft*. jan 2004.

[39] Edward M. Lewandowski. Transverse dynamic stability of planing craft. *Marine Technology and SNAME News*, 34(2):109–118, 1997.

[40] Hui Li, Xuemei Pan, and Chen Guo. SMC for rudder/fin joint roll stabilization based on input-output feedback linearization. *Chinese Control Conference, CCC*, pages 850–855, 2017.

[41] B Liu, Y Jin, A R Magee, L J Yiew, and S Zhang. System identification of Abkowitz model for ship maneuvering motion based on ϵ-support vector regression. In *International Conference on Offshore Mechanics and Arctic Engineering*, volume 58844, page V07AT06A067. American Society of Mechanical Engineers, 2019.

[42] Yasin Masumi and Amir H. Nikseresht. Drag Optimization of A Planing Vessel Based on the Stability Criteria Limits. *China Ocean Engineering*, 33(3):365–372, 2019.

[43] N. Montazeri, S. H. Mousavizadegan, and F. Bakhtiarinejad. The effectiveness of moving masses in reducing the roll motion of floating vessels. *ASME International Mechanical Engineering Congress and Exposition, Proceedings (IMECE)*, 8(PARTS A AND B):101–107, 2010.

[44] Michael G. Morabito. Planing in shallow water at critical speed. *Transactions - Society of Naval Architects and Marine Engineers*, 121(2):636–649, 2015.

[45] Michael G. Morabito. Misbehavioral Analysis. *Professional Boatbuilder*, October/No, 2016.

[46] Michael G Morabito, Aleksandar P Simic, and Antonio B Zgradic. Journal of Ship the Resistance and Trim of Series 50 Experiments. 30(4):153–174, 2014.

[47] Michael Gorts Morabito. Prediction of planing hull side forces in yaw using slender body oblique impact theory. *Ocean Engineering*, 101:47–57, 2015.

[48] Cheol Hoon Park, Hee Chang Park, Han Wook Cho, Seok Jun Moon, and Tae Young Chung. Note: Development of a small maglev-type antirolling system. *Review of Scientific Instruments*, 81(5):1–4, 2010.

[49] T. Perez, N. Smogelif, T. I. Fossenf, and A. J. Sørensen. An overview of the marine systems simulator (MSS): A simulink® toolbox for marine control systems. *Modeling, Identification and Control*, 27(4):259–275, 2006.

[50] Tristan Perez and Graham C Goodwin. Constrained predictive control of ship fin stabilizers to prevent dynamic stall. *Control Engineering Practice*, 16(4):482–494, 2008.

[51] Tristan Perez, Tim Mak, Tony Armstrong, Andrew Ross, and Thor I. Fossen. Validation of a 4DOF manoeuvring model of a high-speed vehicle-passenger trimaran. *9th International Conference on Fast Sea Transportation, FAST 2007*, (September):504–510, 2007.

[52] Andrew Ross, Tristan Perez, and Thor I Fossen. A novel manoeuvering model based on low-aspect-ratio lift theory and lagrangian mechanics. *IFAC Proceedings Volumes*, 40(17):229–234, 2007.

[53] Abdollah Sakaki, Hassan Ghassemi, and Shayan Keyvani. Evaluation of the Hydrodynamic Performance of Planing Boat with Trim Tab and Interceptor and Its Optimization Using Genetic Algorithm. *Journal of Marine Science and Application*, 18(2):131–141, 2019.

[54] M. Y. Santoso, I. Munadhif, A. Wahidin, Ruddianto, Fathulloh, and R. T. Soelistijono. Rudder-roll stabilization using fgs-pid controller for sigma-e warship. *Journal of Physics: Conference Series*, 855(1):0–10, 2017.

[55] Daniel Savitsky. Hydrodynamic design of planing hulls. *Marine Technology*, 1964.

[56] Do Thanh Sen and Tran Canh Vinh. Determination of Added Mass and Inertia Moment of Marine Ships Moving in 6 Degrees of Freedom. *International Journal of Transportation Engineering and Technology*, 2(1):8–14, 2016.

[57] Kuo Ho Su. A roll-motion control system for a mobile-wheeled platform: A preliminary test platform for roll-motion control of ships. *JVC/Journal of Vibration and Control*, 21(14):2796–2812, 2015.

[58] Kazuo Sugai. On the maneuverability of the high speed boat. *Transportation Technical Research Institute, Ministry of Transportation*, pages 1–1057, 1963.

[59] Herve Tanguy, Guy Lebret, and Olivier Doucy. Multi-objective optimisation of pid and H fin/rudder roll controllers. *IFAC Proceedings Volumes (IFAC-PapersOnline)*, 36(21):145–150, 2003.

[60] Oscar Tascón. *Parametrically excited transverse plane instabilities on high speed planing hulls. Michigan*. PhD thesis, 2016.

[61] Sasan Tavakoli and Abbas Dashtimanesh. A six-DOF theoretical model for steady turning maneuver of a planing hull. *Ocean Engineering*, 189(January), 2019.

[62] Sasan Tavakoli, Abbas Dashtimanesh, Simone Mancini, Javad A. Mehr, and Stefano Milanesi. Effects of Vertical Motions on Roll of Planing Hulls. *Journal of Offshore Mechanics and Arctic Engineering*, 143(4):1–10, 2021.

[63] Sasan Tavakoli, Saeed Najafi, Ebrahim Amini, and Abbas Dashtimansh. Ship acceleration motion under the action of a propulsion system: a combined empirical method for simulation and optimisation. *Journal of Marine Engineering and Technology*, (October), 2020.

[64] Mounia Ticherfatine and Zhu Qidan. Nonlinear vertical plan motion feedback stabilization of a fast ferry with flaps and t-foil. In *2016 Chinese Control and Decision Conference (CCDC)*, pages 910–915. IEEE, 2016.

[65] Handa Xi and Jing Sun. Feedback stabilization of high-speed planing vessels by a controllable transom flap. *IEEE Journal of Oceanic Engineering*, 31(2):421–431, 2006.

[66] G. D. Xu, W. Y. Duan, and G. X. Wu. Numerical simulation of oblique water entry of an asymmetrical wedge. *Ocean Engineering*, 35(16):1597–1603, 2008.

[67] G. D. Xu, W. Y. Duan, and G. X. Wu. Simulation of water entry of a wedge through free fall in three degrees of freedom. *Proceedings of the Royal Society A: Mathematical, Physical and Engineering Sciences*, 466(2120):2219–2239, 2010.

[68] H. Yasukawa, R. Sakuno, and Y. Yoshimura. Practical maneuvering simulation method of ships considering the roll-coupling effect. *Journal of Marine Science and Technology (Japan)*, 24(4):1280–1296, 2019.

[69] Hironori Yasukawa and Yasuo Yoshimura. Roll-coupling effect on ship maneuverability. *Ship Technology Research*, 61(1):16–32, 2014.

[70] Ernest E Zarnick. A non-linear mathemathical model of motions of a planning boat in regular waves. *Tech. Rep. DTNSRDC- 78/032, David Taylor Naval Ship Reasearch and Development Center, Bethesda, Md, USA*, 1978.

[71] Hamid Zeraatgar, Aliasghar Moghaddas, and Kazem Sadati. Analysis of surge added mass of planing hulls by model experiment. *Ships and Offshore Structures*, 15(3):310–317, 2020.

Appendix A

MATLAB MODEL CODE REFERENCE

Electronic repository of model files are at: https://github.com/sung2799/planing-hull

This section contains a description of the MATLAB files developed to perform the modeling, simulation, and analysis in this paper. In order to run a full simulation, you will need all files contained in the Github repository in your MATLAB working folder since the files contain functions that have inter-dependencies. Description of files are grouped by functionality:

High level functions and integrators for full simulations

- `simroll4DOF`: Simulates an open loop trajectory in 4DOF. This can be run to determine stable equilibrium states. Input requested parameters such as run time, initial conditions, fixed mass lateral position and rudder position, etc... Save output file to be used as an input file for used by `Robust_LQR_MIMO` for closed loop control and analysis.

- `Robust_LQR_MIMO`: Creates optimal closed loop feedback control systems about the equilibrium established by `simroll4DOF`. A sample file is included in the repository for demonstration. Performs linear analysis of closed loop systems of AMA, Rudder, and composite AMA and rudder systems, as well as open loop and closed loop simulation.

Provides hydrodynamic force estimates

- `roll_dynamic_4DOF_NL18`: Models hydrodynamic forces to enable non-linear time domain simulation.

- `lin_interpsys4`: Models hydrodynamic forces to enable Jacobian for linearization.

- `interp_point`: Produces the interpolated hydrodynamic forces given a single state point. This function queries the data output from `interp_model` to give force estimates.

Input, output, and enabling functions

- `sim_setup`: Contains vessel geometries, particulars and input parameters
- `t0_solver`: Routine that calculates steady state trim using Savitsky classic method, reference section 2.2
- `MIMO`: Numerically linearizes a MIMO system by Jacobian. Uses `lin_interpsys4` as the engine to produce hydrodynamic force models about a given equilibrium
- `SISO_LQR`: Numerically linearizes a SISO system. Also uses `lin_interpsys4`
- `Draw`: Creates figures and analysis output
- `Video`: Animates a trajectory on a X-Y plot from simulation output variable
- `interp_model`: Draws from experimental results data file, performs a coordinate reference change to measurement axes from wind axes, calculates Delaunay triangulation and outputs the simplex lookup data tables required to interpolate in n-dimensions.
- `data_interp2`: Data file of experimental results in wind axes, used by `interp_model`.

For any questions or concerns, I welcome your feedback at: sung2799@gmail.com

Appendix B

SYSTEM ID VIA MODAL DECOMPOSITION

Traditionally, test data such as produced by a Planar Motion Mechanism (PMM) would evaluated forces on a linear basis proportional to the time derivatives of state parameters. However, the nonlinear nature of planing vessels deem that such an approach is only accurate near the state that the test measurement was taken as noted by (Judge & Judge, 2013). In addition, we seek to determine the sensitivity to non-state parameters, such as vessel deadrise and wetted water lengths. This necessitates other means to extract a closed form model and data methods that are able to simplify complex non-linear processes. Our approach is to first apply Singular Value Decomposition (SVD), use dominant parameters to form candidate model equations, and use a least squares method to identify best fits to these equations and their coefficients.

Performing SVD yields valuable clues regarding the hydrodynamic force dependencies on state parameters such as roll, sway, trim, wetted water lengths for a particular vessel hull type, as well as geometrically related parameters such as deadrise. This information can advise test libraries of candidate equations to least squares fit with data. Finally, a sparsity filter, such as developed by Brunton (2015) could eliminate terms of least dependency. The value of such a method lies in the ease of application, scalability up to the extent of available data, and the ability to simplify down to meet the desired computational expenditure for this task.

B.1 Results of Singular Value Decomposition

The data is assembled so that applicable parameters are associated with the force to be modeled. This consists of geometric and state parameters of deadrise, trim, roll angle, and

sway velocities. Even though our model system is not free to rotate in pitch, steady state trim values is a considered input parameter. In addition, based on Judge (2013), we also include wetted chine lengths port, starboard, sum of wetted chine lengths, and the difference.

$$\theta(X) = \begin{bmatrix} DR & \tau_0 & \phi & v & lc_p & lc_s & \Sigma lc & \Delta lc \end{bmatrix} \tag{B.1}$$

SVD is performed on normalized data. The forces can be represented in 5 modes.

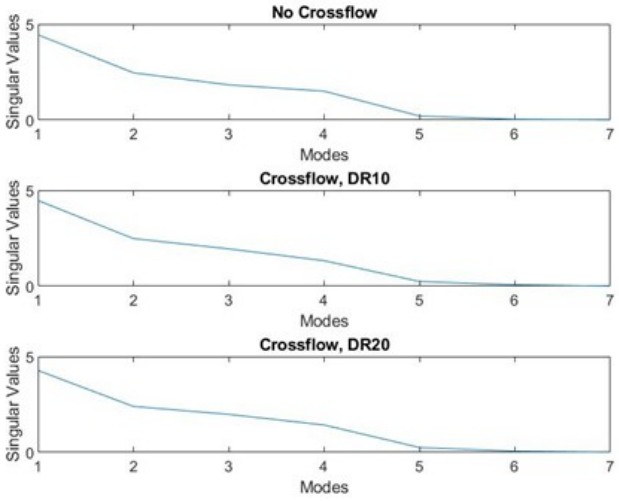

Figure B.1: Modal decomposition

Data of tests with and without sway and with deadrise of 10 and 20 degrees shown to primarily consist of 5 modes. A multiplication of those modes with the left singular values provides a general idea of the parameter dependencies.

Correlation of hydrodynamic force on parameters as indicated by singular values. Data presented in conditions with and without crossflow with deadrises of 10 and 20 degrees.

SVD results show the relative importance of available parameters to hydrodynamic forces. For tests of straight trajectories without obliquely towed angle or crossflow, dominant terms

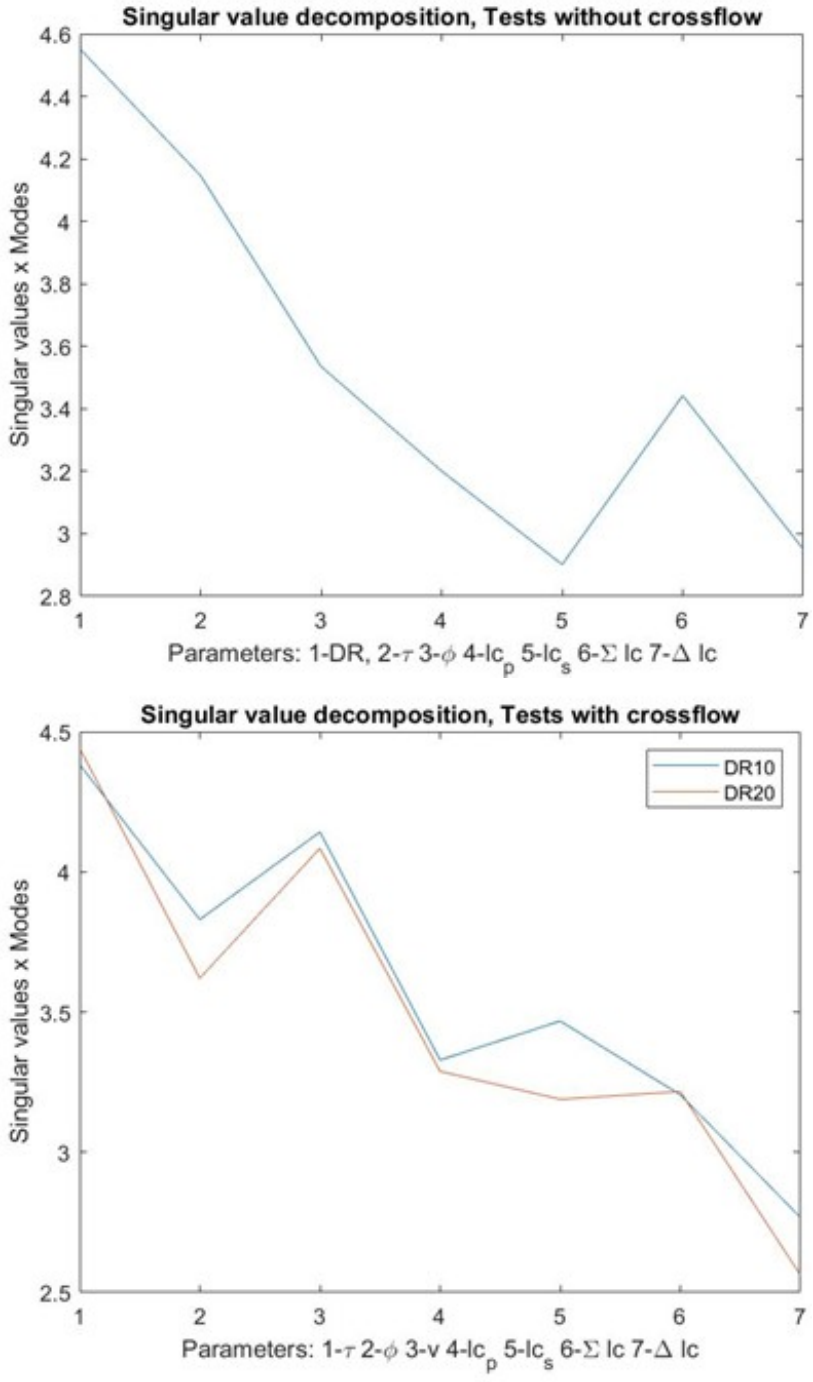

Figure B.2: Relative parameter dependencies

of Deadrise, Trim, Heel, Σlc (sum of wetted chine lengths) account for 62% of dynamic system energy. For obliquely towed tests with crossflow, 50% of system energy is contained with trim, heel, and apparent crossflow. As we would expect from theory, the most dominant terms are deadrise, τ, and heel angles, and Σlc; this corroborates well with our understanding of planing vessel dynamics. Faltinsen [21] relates lift force with τ. Perez [51] presents a "wing theory" with two sides of the hull, port and starboard, as dihedral wings with lift as a function of trim. The apparent angle of attack of each wing are then functions of the vessel's geometric deadrise parameter, as well as trim and heel. This presents a useful conceptual presentation to the force variations due to deadrise, τ, and heel angles. [31] establishes the value of wetted chine length in modeling roll dynamics.

B.2 Empirical Model Development

An empirical model formulation was attempted but not used for the results contained in this paper. While it yielded positive results for certain vessel conditions, the model did not accurately capture the dynamics in all. The methods here show promise, but we are constrained due to the lack of high fidelity time dependent test data. However, it is worthy to note the processes used, since a universally applicable empirical model for coupled planing dynamics would enhance the range of usable conditions beyond the interpolative approach shown in this paper.

Based on SVD and a basic understanding of the dependency of hydrodynamic forces to geometric and state parameters, we propose equations and evaluate their fit to data. Our goal is to extract a set of governing equations from the data using sparsity-promoting techniques described by Brunton [10]. We propose a set of candidate functions that would span the data space to establish governing equations. They consist of exponential terms, cross terms, and trigonometric functions.

$$\theta(\nu) = \begin{bmatrix} DR & \tau_0 & \phi & v & lc_p & lc_s & \Sigma lc & \Delta lc \end{bmatrix} \tag{B.2}$$

$$\Theta = \begin{bmatrix} 1 & \sqrt{\theta} & \theta & \phi v & \phi \Sigma lc & \frac{sin(\phi)}{sin(DR)} & \frac{sin(\tau_0)}{sin(DR)} \end{bmatrix} \tag{B.3}$$

$$\Xi = (\Theta' \Theta)^{-1} \Theta \tag{B.4}$$

To determine the best coefficients for the candidate function terms, we employ least squares fit to sway force Y and yaw moment N data. Moore-Penrose inverse functions are utilized in the least squares calculations to avoid singularities.

$$Y_{est} = \Xi_Y S \tag{B.5}$$

$$N_{est} = \Xi_N S \tag{B.6}$$

We organize the candidate functions in libraries. The first consists of SVD identified dominant terms, the second of polynomial terms up to 2nd order of all parameters, and the third of cross terms of all parameter combinations to 2nd order. Library three is a combination of libraries one and two, and library four included all terms above mentioned to yield 81 terms. Seeking to determine the fewest terms to accurately represent the data, these libraries are run through a sparsity filter developed by [11]. This method is based on an efficient least squares algorithm and application of a term by term comparison to a set threshold, then fit with least squares method to the data, and compared with R squared values.

Parameter dependencies shown with and without crossflow with deadrise of 10 and 20 degrees. This demonstrates a low cost method to extract physically intuitive closed form models of complex systems. Note, our model data is based on steady state measures and does not capture time dependencies. Our model does not consider hydrodynamic force changes due to time derivatives of state. However, the process is scalable to much larger data sets. Higher accuracy can be obtained with full state time varying data of non-captive models in high speed maneuver. With the low computing resource requirement of this method, it may be possible to develop a model in real time with onboard vessel sensors combined with a machine learning algorithm to develop highly accurate models for model predictive control, which is a potential direction for this work.

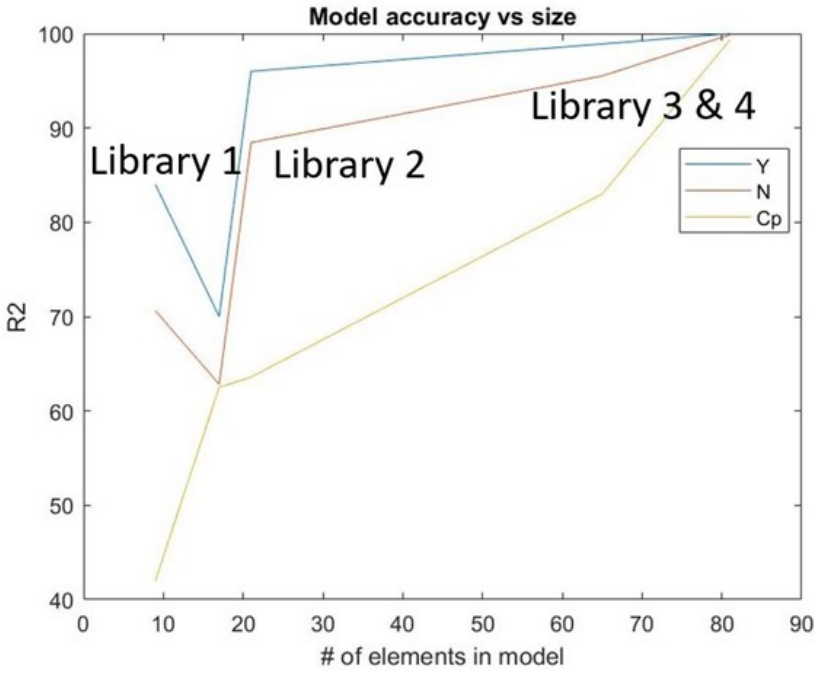

Figure B.3: Candidate library evaluation

To explore coupled dynamics and new methods of control, we obtained closed form model by combining SVD determined dominant terms in a combination of twelve fifth order cross terms. Figure 5 shows that libraries with physical information resulted in a quicker convergence for Y and N than the other libraries which were run without. Library 1, consisting of SVD identified dominant parameters performed more effectively per term than indiscriminant parameter libraries, as we would expect. This process demonstrated stronger performance in the modeling of sway force Y and yaw moment N than Cp, indicating at further hydrodynamic analysis may be required in determining the factors impacting the location of forces acting on the hull.

The sparsity filtering process revealed that the data had relatively low fidelity. It lacked sparsity and indicated that near all of the candidate terms held modeling value. Additional parameters would be needed for the sparsity filtering process to work as intended. Eight parameters (deadrise, trim, roll, etc...) for each test run is a relatively small number of

inputs to model maneuver forces with. Full scale measurements in free running tests would yield greater data and ability to evaluate other hydrodynamic parameters to improve the model. Nevertheless, using this process on our model dataset yielded R squared values of 95% for Y and 92% for N which represents a balance between accuracy and model complexity given our data limitations, while avoiding overfitting. It is sufficient for initial analysis and control design.

Appendix C

MATLAB SUPPLEMENTAL - DYNAMICS

This captures the basic MATLAB code of the 5DOF nonlinear dynamic model

```
%5DOF: Surge(u),Sway(v),Roll(F),Yaw(S),Actuator

function dy = roll_dynamics_4DOF_NL18(y,XX,YY,tri,lcg,vcg,zm,DR
,ma,mb,A,B,t0,U0,int,I,CL) % open loop

%Universal constants
pw=1.92; g=32.2;
F=y(3);
S=y(4);
u=y(5);
v=y(6);
p=y(7);
r=y(8);
d1=y(9); %Actuator states (d1-position, d2-velocity)
d2=y(10);
XI=[DR t0 v r F];

U_r=U0(3); U_x=U0(1); U_p=U0(4);  %Establishes input channels, including for
disturbance

[Yint]= interp_point(XX,YY,tri,XI,int); %XI=[DR t0 v r F]
```

```
%% Rudder model
SL=atand(v/u);
AoA=U_r-SL;
L=.5*(.0018)*u^2*AoA;
Y_rud=L;
X_rud=-.5*(4.6e-5*AoA^2+1.38e-4*abs(AoA)+9.2e-4)*u^2;
K_rud=-Y_rud*z_rud;
N_rud=-Y_rud*lcg;

%% Forces
Ix=A(3,3)+ma*(d1^2+zm^2); %Dynamic roll moment of inertia
A2=A; A2(3,3)=Ix;

C_X=U_x+X_rud; %setting thrust = drag for constant velocity
C_Y=Y_rud; %sway from rudder
C_K=K_rud+U_p; % roll force from control mass & disturbance input
C_N=N_rud;
C_d2=F_a;

F_hd=Yint';
F_co=[C_X;C_Y;C_K;C_N];
loa=50/12; Iy=mb*(.25*loa)^2;
yg=0; xg=0; q=0;

Cor=[0 0 mb*yg*q*(pi/180)^2 -mb*(xg*r*(pi/180)^2+v*(pi/180));        %X
    0 0 -mb*yg*p*(pi/180)^2 -mb*(yg*r*(pi/180)^2-u*(pi/180));        %Y
    -mb*yg*q*(pi/180) mb*yg*p*(pi/180) 0 -Iy*q*(pi/180)^2;         %K
```

```
    mb*(xg*r*(pi/180)+v) mb*(yg*r*(pi/180)-u) Iy*q*(pi/180)^2 0];  %N

RM=[cosd(S) -sind(S) 0 0;
    sind(S) cosd(S) 0 0;
    0  0 1 0;
    0 0 0 1];

% Equation of motion
dy=[zeros(4) RM zeros(4,2); zeros(4) -A2\B zeros(4,2); zeros(2,10)]*y...
    +[zeros(4,8) zeros(4,2);zeros(4) -A2\Cor zeros(4,2); zeros(2,10)]*y...
    +[zeros(4,1);A2\(F_hd+F_co);0;ma\C_d2];

dy(7)=dy(7)-ma/Ix*(2*d1*d2*p+zm*d1*p^2-g*d1*cosd(F));  %pd - actuator dynamics
dy(9)=d2;   %controller velocity defined
dy(10)=dy(10)+d1*p^2+g*sind(F)-zm*dy(7); %controller d dynamics
dy(5)=0; %set X direction acceleration to 0

if CL==0  %if Open Loop, freeze position of control mass
dy(10)=0;
end
warning('off')
```

Appendix D

MATLAB SUPPLEMENTAL - INTERPOLATION SETUP

This imports the raw data from Brown and Klosinski captive tests [8] for a turn to starboard in wind axes, performs coordinate transformation to measurement axes, models the forces that would be experienced by a free running model vice captive test by adjusting for a free running lcg, extrapolates model values for a turn to port based on vessel symmetries, rounds the values, performs Delaunay triangulation and exports the simplices.

```
function [XX,YY,tri]= interp_model(lcg)

%% Setup interpolation model
% D_b = xlsread('data_interp2.xls',2,'A2:J97'); %sheet 2 for body axes data
D_w = xlsread('data_interp2.xls',1,'A2:J177');

% Establish measurement axes data
Xw=D_w(:,7);
Yw=D_w(:,8);
Kw=D_w(:,9);
Nw=D_w(:,10);
SS=D_w(:,3);  %side slip angle

for j=1:length(D_w)
XYm(:,j)=[cosd(SS(j)) sind(SS(j)); -sind(SS(j)) cosd(SS(j))]\[Xw(j); Yw(j)];  %rotation
Km(j)=Kw(j)/cosd(SS(j));
Nm(j)=Nw(j)-(-1.875+lcg)*Yw(j);
```

```
end
Xm=-XYm(1,:)'; Ym=XYm(2,:)'; Km=Km'; Nm=Nm';
D_m=[D_w(:,1:6) Xm Ym Km Nm];

E_m=D_m; %Extrapolation Model (based on symmetric v,r,F,Y,K,N)
E_m(:,4)=-E_m(:,4); %v
E_m(:,5)=-E_m(:,5); %r
E_m(:,6)=-E_m(:,6); %F
E_m(:,8)=-E_m(:,8); %Y
E_m(:,9)=-E_m(:,9); %K
E_m(:,10)=-E_m(:,10); %N
D_m=[D_m;E_m];
XX=[D_m(:,1:2) D_m(:,4:6)]; %side slip angle removed since not needed
X=D_m(:,7); Y=D_m(:,8); K=D_m(:,9); N=D_m(:,10);
XX_m=XX; K_m=K; Y_m=Y; X_m=X; N_m=N;
save('D_m.mat','XX_m','K_m','Y_m','X_m','N_m');
% YY=[X Y K N];  %Raw Force vector

[XX,~,ind2] = unique(XX,'rows');
YY_X = accumarray(ind2,X,[size(XX,1),1],@mean); % YY_X=X(ind1);
YY_Y = accumarray(ind2,Y,[size(XX,1),1],@mean); % YY_Y=Y(ind1);
YY_K = accumarray(ind2,K,[size(XX,1),1],@mean); % YY_K=K(ind1);
YY_N = accumarray(ind2,N,[size(XX,1),1],@mean); % YY_N=N(ind1);
YY=[YY_X,YY_Y,YY_K,YY_N];  %averaged force vector

tri = delaunayn(XX);
```

Appendix E

MATLAB SUPPLEMENTAL - INTERPOLATE POINT

Given a state, provides interpolated force estimates. Two methods are provided. 1) using MATLAB internal function "griddatan" and 2) our method which pulls from pre-calculated simplices and reduces computation cost, reference 4.1

```
% Requires: XI, lcg, DR, sim_setup, & interp_model(lcg) for XX,YY,tri

function [Yint]= interp_point(XX,YY,tri,XI,int) %XI=[DR t0 v r F]

%%
% format for XI=[DR t0 v r F];

if int==1  % allows for use of MATLAB internal interpolator - much slower method
load('D_m.mat','XX_m','X_m','Y_m','K_m','N_m')
X = griddatan(XX_m,X_m,XI);
% Y=0; %Y model with linear damping matrix
Y = griddatan(XX_m,Y_m,XI); %Y test data yields unintuitive results
K = griddatan(XX_m,K_m,XI);
N = griddatan(XX_m,N_m,XI);
Yint=[X Y K N];
end

if int==2  % our script utilizes a single simplex calculation - much faster
[t,p] = tsearchn(XX,tri,XI);
```

```
YY_X=YY(:,1); YY_Y=YY(:,2); YY_K=YY(:,3); YY_N=YY(:,4);
X = p*YY_X(tri(t,:));
Y = p*YY_Y(tri(t,:));
K = p*YY_K(tri(t,:));
N = p*YY_N(tri(t,:));
Yint=[X Y K N];

end
```

Appendix F

MATLAB SUPPLEMENTAL - LINEARIZATION BY NUMERICAL JACOBIAN

Numerically performs Jacobians to attain linearized system dynamics. Forces are assess given perturbations about an equilibrium point in each state direction, then divided by the value of that perturbation, reference 6.1.

```
function [AA,BB] = MIMO(x0,XX,YY,tri,lcg,vcg,zm,DR,ma,mb,A,B,t0,U0,I,int,CL)
% 5DOF actuator dynamics
e=x0(3:10,1);
dD=.1;
[dx,dx_c] = lin_interpsys8(e,XX,YY,tri,lcg,vcg,zm,DR,ma,mb,A,B,t0,U0,int,I,CL);

%AA - linearized system dynamics (AA matrix)
AA=zeros(8,8);
for j=1:8
e2=e; e2(j)=e(j)+dD;
[dx2,~] = lin_interpsys8(e2,XX,YY,tri,lcg,vcg,zm,DR,ma,mb,A,B,t0,U0,int,I,CL);
AA(:,j)=(dx2-dx)/dD;
end

U2=U0; U2(2)=U0(2)+dD; % Input - mass
[~,dx_c2] = lin_interpsys8(e,XX,YY,tri,lcg,vcg,zm,DR,ma,mb,A,B,t0,U2,int,I,CL);
BB(:,1)=(dx_c2-dx_c)./dD;
```

```
%BB - linearized control dynamics
U2=U0; U2(3)=U0(3)+dD; % Input - rudder
[~,dx_c2] = lin_interpsys8(e,XX,YY,tri,lcg,vcg,zm,DR,ma,mb,A,B,t0,U2,int,I,CL);
BB(:,2)=(dx_c2-dx_c)./dD;

U2=U0; U2(4)=U0(4)+dD; % Input - roll disturbance
[~,dx_c2] = lin_interpsys8(e,XX,YY,tri,lcg,vcg,zm,DR,ma,mb,A,B,t0,U2,int,I,CL);
BB(:,3)=(dx_c2-dx_c)./dD;
```

Appendix G

MATLAB SUPPLEMENTAL - TRIM ANGLE ESTIMATE

Uses Savitsky method to estimate steady trim angle. 2.2

```
function [t0] = t0_solver(b,g,Cv,lcg,pw,u,DR,mb)

% solve for SS trim and wetted waterline using savitsky methods
%Solver for lw (at steady state, lp = lcg)
F = @(lw) lw*b*(.75-(5.21*Cv.^2/lw.^2+2.39).^(-1))-lcg; %lw - non dimensional wetted wat
x0=1.7;
[lw,fval]=fsolve(F,x0);

% Solver for Cl0 using Savitsky SS methods
Clb=mb*g/(.5*pw*u^2*b^2);
F = @(Cl0) Clb-Cl0+.0065*DR*Cl0.^.6;
x0=.14;
[Cl0,fval]=fsolve(F,x0);

% % SS estimate of tau
%lw=3;
F = @(t0) -Cl0+(t0).^1.1*(.012*lw.^.5+.0055*lw.^2.5/Cv^2);
x0=5;
%options=optimoptions('fsolve','Display','iter');
[t0,fval]=fsolve(F,x0);
```

```
F = @(x) .89+(1.4/x)*(1-x^2)^.5;
x0=10;
%options=optimoptions('fsolve','Display','iter');
[x,fval]=fsolve(F,x0);
```

VITA

After graduating from the University of California, San Diego with a Bachelors Degree in Mechanical Engineering in 1999, Li joined the Navy. He served worldwide as an engineer and a diver, and was selected into the Permanent Military Professor program in 2017. Following the University of Washington, Li will be serving as an educator of future officers at the United States Naval Academy in the Department of Naval Architecture and Ocean Engineering. He will be accompanied by his wife, Ione, and two daughters, Iona and Tayana.